Inferred influence of nutrient availability on the relationship between Sun-induced chlorophyll fluorescence and incident irradiance in the Bering Sea

Christina Schallenberg,[1] Marlon R. Lewis,[1] Dan E. Kelley,[1] and John J. Cullen[1]

Received 22 May 2007; revised 21 April 2008; accepted 5 May 2008; published 30 July 2008.

[1] This study examines variability in the relationship between Sun-induced chlorophyll fluorescence and incident solar irradiance as a potential diagnostic of the nutritional status of phytoplankton. The study site is the Bering Sea, where two optical drifters were caught for more than 100 days in an anticyclonic eddy, while two others provided data from adjacent waters. Estimates of fluorescence emission normalized to the absorption of light by pigments were analyzed as a function of irradiance to describe variability of the quantum yield of fluorescence. Yields in bright sunlight and under lower light varied by a factor of 5 or more on the scale of days to weeks. For the one drifter that remained in the high-velocity region of the eddy, there was a lagged correlation between the eddy rotation period and fluorescence parameters, with higher fluorescence yields in both low and high irradiance associated with slower rotation. Since nutrient input to the photic zone may increase with increasing shear of the eddy flow, this is consistent with the established suggestion that Sun-induced fluorescence increases with nutrient stress in phytoplankton. Independent measurements of variable fluorescence (*Fv*/*Fm*, an indicator of photosynthetic efficiency) further support this interpretation. However, modeling shows that the established hypothesis of competition between photosynthesis and fluorescence for absorbed photons (i.e., photochemical quenching), with high fluorescence yields reflecting photosynthetic debility, does not apply near the sea surface, where photosynthesis is saturated, and dissipation of excess absorbed radiation by nonphotochemical quenching is the dominant influence on fluorescence yield.

Citation: Schallenberg, C., M. R. Lewis, D. E. Kelley, and J. J. Cullen (2008), Inferred influence of nutrient availability on the relationship between Sun-induced chlorophyll fluorescence and incident irradiance in the Bering Sea, *J. Geophys. Res.*, *113*, C07046, doi:10.1029/2007JC004355.

1. Introduction

[2] Global fields of chlorophyll *a* concentration derived from satellite observations of ocean color reveal broad patterns that show the strong influence of physical processes on primary productivity through the transport of nutrients to the photic zone [*Sverdrup*, 1955; *Williams and Follows*, 2003; *McGowan*, 2004]. In addition to biogeographical patterns related to ocean circulation [*Yentsch and Garside*, 1986; *Longhurst*, 2007], much variability is found on the mesoscale, with spatial scales on order of 10–100 km and timescales on order of 10–100 days [*Lewis*, 2002; *Longhurst*, 2007]. It has been suggested that mesoscale eddies influence primary productivity by enhancing nutrient supply to the euphotic zone by a number of mechanisms [e.g., *Tranter et al.*, 1980; *Yentsch and Phinney*, 1985; *Falkowski et al.*, 1991; *Martin and Richards*, 2001; *Lévy*, 2003; *McGillicuddy et al.*, 2007], and it has been found that photosynthetic parameters of the phytoplankton community could be related to the physical structure and dynamics of meanders and eddies [e.g., *Lohrenz et al.*, 1993]. However, while satellite estimations of chlorophyll can show where net growth of phytoplankton has occurred, they hold no direct information on the photosynthetic capabilities of phytoplankton (but see *Behrenfeld et al.* [2005]). Physiological assessment of phytoplankton from space would make it much easier to quantify the relationships between physical forcing, the nutrient status and growth rates of phytoplankton, ecosystem structure and biogeochemical cycling in the sea.

[3] Remote detection of radiance in red wavelengths originating from Sun-induced chlorophyll fluorescence near the ocean surface may provide insights into phytoplankton dynamics, because fluorescence yield is functionally related to photosynthesis and varies as a function of physiological status [*Falkowski and Kiefer*, 1985; *Kiefer et al.*, 1989; *Chamberlin et al.*, 1990; *Babin et al.*, 1996; *Letelier et al.*, 1997, 2000; *Laney et al.*, 2005]. Observations of Sun-induced chlorophyll fluorescence (SICF; also called natural fluorescence) near the sea surface reveal considerable var-

[1]Department of Oceanography, Dalhousie University, Halifax, Nova Scotia, Canada.

0148-0227/08/2007JC004355

iability in space and time that may reflect environmental controls on the photosynthesis and physiological status of phytoplankton [*Letelier et al.*, 1997; *Abbott et al.*, 2001]. For example, satellite-borne Moderate-Resolution Imaging Spectroradiometer (MODIS) imagery of fluorescence line height normalized to chlorophyll *a* and similar data products reveal patterns that are well related to hydrographic features and thus are likely to be environmentally forced, but the underlying processes are poorly understood [*Huot et al.*, 2005].

[4] The emission of fluoresced photons from phytoplankton is generally expressed as a function of incident irradiance, the absorption of light by phytoplankton, and the quantum yield of fluorescence, ϕ_f, which is the ratio of photons emitted from chlorophyll molecules as fluorescence to those absorbed by the cell [*Falkowski and Kiefer*, 1985; *Kiefer et al.*, 1989]. This operational definition of ϕ_f is not restricted to absorption of light by the source of fluorescence, primarily photosystem II, so it is not identical to the physiological quantum yield [*Gilmore and Govindjee*, 1999]. Laboratory studies using so-called natural [*Laney et al.*, 2005] or stimulated fluorescence measurements show that metrics or proxies of the quantum yield of fluorescence are influenced by the nutritional status of phytoplankton [e.g., *Kiefer*, 1973a; *Cleveland and Perry*, 1987; *Abbott et al.*, 2000]; field measurements using both passive and stimulated measurements of fluorescence support this finding [*Kiefer*, 1973b; *Letelier et al.*, 1997; *Abbott et al.*, 2000; *Letelier et al.*, 2000]. However, the use of the remotely sensed fluorescence signal as a diagnostic for nutrient stress is complicated by the fact that phytoplankton near the surface can experience acute physiological stresses due to excessive irradiance as well as nutrient limitation [e.g., *Babin et al.*, 1996], and the combined effects of these stresses on the fluorescence quantum yield under full sunlight are poorly understood [*Cullen and Lewis*, 1995; *Cullen et al.*, 1997; *Laney et al.*, 2005]. For example, it has been shown [*Maritorena et al.*, 2000; *Morrison*, 2003] that under excess irradiance near the sea surface, the fluorescence quantum yield is subject to so-called nonphotochemical quenching, a diversion of absorbed energy to nonfluorescent sinks, i.e., enhanced dissipation as heat [*Krause and Weis*, 1991; *Müller et al.*, 2001]. Very little is known, however, about the effects of nutrient limitation on nonphotochemical quenching [*Laney et al.*, 2005].

[5] In their analysis of data from an optical drifter in an eddy in the Southern Ocean, *Letelier et al.* [1997] defined an apparent fluorescence quantum yield as the slope of the relationship between FLH/chl (fluorescence line height normalized to the concentration of chlorophyll, as estimated using ocean color measurements from the drifter) and the incident irradiance at 490 nm. They related a time series of this apparent ϕ_f to the inferred supply of nutrients to the euphotic zone of the eddy and concluded that high fluorescence yields were related to nutritional deficiency, and vice versa. The hypothesis is that fluorescence and photosynthesis compete for absorbed photons (i.e., fluorescence yield is reduced by the process called photochemical quenching [*Kiefer and Reynolds*, 1992]), and photosynthetic debility leads to decreased photochemical quenching and thus increased fluorescence quantum yield. In another study of fluorescence yield as measured by drifters in the Southern Ocean, *Abbott et al.* [2001] related high fluorescence yield to photosynthetic stress induced by either light or nutrients. Neither analysis of fluorescence measured by drifters explicitly considered nonphotochemical quenching, in which the quantum yields of both fluorescence and photosynthesis are reduced as absorbed photons are dissipated as heat in response to excess irradiance [*Krause and Weis*, 1991; *Müller et al.*, 2001].

[6] *Letelier et al.* [1997] concluded that SICF quantum yield may prove to be a useful diagnostic of nutrient stress and that, with more research, it might be used for remote sensing of the influence on phytoplankton growth of variability in the supply of nutrients to the euphotic zone. Subsequently, methods for parameterizing SICF have improved, and a greater appreciation of the importance of nonphotochemical quenching has developed [*Maritorena et al.*, 2000; *Morrison*, 2003; *Huot et al.*, 2005; *Laney et al.*, 2005]. Still, fundamental questions remain about the relationships between near-surface SICF and the nutrition of phytoplankton [*Laney et al.*, 2005]. For example, in their theoretical analysis, *Babin et al.* [1996] assumed that nutrient stress would increase the susceptibility of phytoplankton to excess irradiance, leading to inactivation of reaction centers and reduced fluorescence yield, comparable to nonphotochemical quenching. It is worth noting that the effect of nutrition on near-surface fluorescence yield assumed by *Babin et al.* [1996] is the opposite of that invoked by *Letelier et al.* [1997].

[7] Following the general approach of *Letelier et al.* [1997], we analyzed Sun-induced fluorescence observations taken from four drifting buoys equipped with optical sensors and deployed for >100 days within and out of an anticyclonic eddy in the Bering Sea in an effort to discern physiologically interpretable variations in fluorescence yield in response to inferred variability of nutrient supplies associated with oceanographic forcing. Our analysis goes beyond that of *Letelier et al.* [1997] by resolving changes beyond the initial slope of the fluorescence-irradiance relationship, thus taking nonphotochemical quenching into account [*Morrison*, 2003; *Laney et al.*, 2005]. Furthermore, we normalized the fluorescence signal to absorption rather than to chlorophyll *a* and corrected it for attenuation of light in the water column, thereby allowing direct estimation of quantum yield; both corrections have been shown to be important for the analysis of the fluorescence signal [*Cleveland and Perry*, 1987; *Babin et al.*, 1996; *Culver and Perry*, 1997; *Huot et al.*, 2005]. Finally, we were able to sample water from the eddy being monitored by the drifter to obtain independent physiological assays [*Parkhill et al.*, 2001] for evaluating the link between Sun-induced fluorescence yield and the nutrition of phytoplankton. This more comprehensive analysis found the same relationship between inferred nutrient stress in phytoplankton and increased quantum yield of near-surface Sun-induced chlorophyll fluorescence as described by *Letelier et al.* [1997]. However, our analysis of fluorescence yield as a function of irradiance shows a dominant influence of nonphotochemical quenching, thereby eliminating the working hypothesis of *Letelier et al.* [1997] (also used by *Abbott et al.* [2001] and our own research group when we began our analysis), which invokes photochemical quenching as an

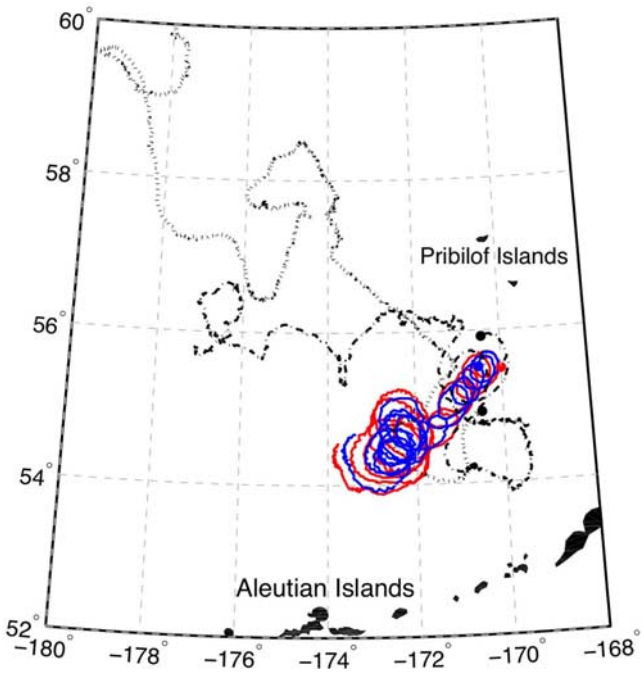

Figure 1. Tracks of the four drifters in the Bering Sea. While two drifters were clearly traveling with the eddy (blue, eddy 1; red, eddy 2), the other two drifters traveled on trajectories outside the eddy (dash-dotted line, control 1; dashed line, control 2).

explanation for the relationship between nutrient stress and high fluorescence yield at the sea surface.

2. Data and Methods

2.1. Instruments and in Situ Measurements

[8] We analyzed data from four drifters, deployed in June 1997 in the eastern Bering Sea between 54° and 56° N and 170° and 170.5° W (Figure 1). The World Ocean Circulation Experiment (WOCE)-type drifters (METOCEAN Data Systems Inc.) were drogued at 40 m with a holey sock drogue; the surface float contained a multichannel sensor (Satlantic Inc.) [see *Landry et al.*, 1997] to measure the upwelling radiance, $L_u(\lambda)$ (μmol quanta m^{-2} s^{-1} nm^{-1} sr^{-1}), at seven wave bands (412, 443, 490, 510, 555, 670, and 683 nm) 10–15 cm below the sea surface, a single wave band sensor to measure the above-water downwelling irradiance at 490 nm, $E_d(490, 0^+)$ (μmol quanta m^{-2} s^{-1} nm^{-1}), and a thermistor to measure sea surface temperature. The spectral response curves of the optical sensors have a bandwidth of 10 nm at half-maximum, narrower than the 20-nm bandwidth of the sensors on the Sea-viewing Wide Field-of-view Sensor (SeaWiFS) instrument in the visible bands.

[9] The four drifters were deployed on the edge of an eddy that had been previously identified using TOPEX/POSEIDON altimetry and shipboard conductivity-temperature-depth (CTD) transects. All drifters logged optical observations on an hourly basis during the day, and transmitted these data, along with sea surface temperature, via the ARGOS satellite communications network. Two drifters, 29064 and 29068, here referred to as eddy 1 and eddy 2, traveled with the eddy while the other two, 29063 and 29067, referred to as control 1 and control 2, followed trajectories outside the eddy (Figure 1).

[10] The eddy was further surveyed as it moved southwestward, hydrographically using a CTD (Figure 2), and optically using a profiling multichannel radiometer (SPMR, Satlantic Inc.) and a tethered multichannel radiometer buoy (OCP-100, Satlantic Inc.), during an accompanying cruise in the Bering Sea from 11 to 26 June 1997 aboard the R/V *Wecoma*. The SPMR profiler measured $E_d(\lambda, z)$, downwelling irradiance at depth z (m), at 13 wavelengths. The OCP-100 carried two, 14-channel sensors to measure: (1) $L_u(\lambda)$, upwelling radiance, 20 cm below the surface, and (2) $E_d(\lambda, 0^+)$, downwelling irradiance above the sea surface, sampling at 6 Hz. The analyses presented here are based on 1-min medians from deployments of the OCP-100 at stations over the Bering Sea slope and shelf.

[11] Highly spectrally resolved optical measurements from the Bering Sea in 2000 and 2001 were used to develop and evaluate methods for estimating the photosynthetically available radiation (PAR) from the $E_d(490, 0^+)$ measurements of the optical drifters, and also to derive a robust correction for backscattered solar radiation contributing to the upwelling radiance at 683 nm. Measurements were made with a Satlantic Hyperspectral Tethered Spectral Radiometer Buoy (Hyperspectral TSRB) that measured downwelling irradiances and upwelling radiances at 123 wavelengths. The upwelling sensor measured at 70 cm below the surface and downwelling irradiance was measured above the surface. The spectral response curves of the instrument have a bandwidth of 10 nm at half-maximum and the measurements are thus comparable to those from the drifters. For each deployment of the instrument, the medians of about 40 measurements recorded during the last minute of deployment were used to represent spectra of downwelling irradiance and upwelling radiance.

2.2. Discrete Samples

[12] Samples of near-surface phytoplankton were collected with a clean polyethylene bucket during deployments of the

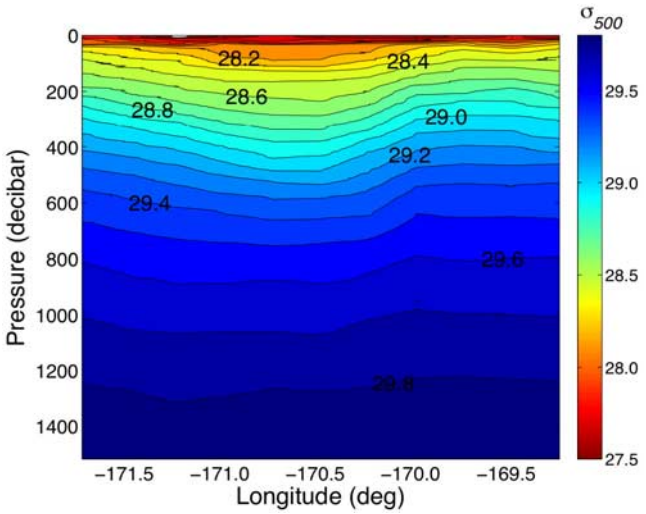

Figure 2. Contours of density anomaly (σ_{500}) from a representative east-west conductivity-temperature-depth transect through the eddy on 23–24 June 1997. Pressure in decibars is a proxy for depth in meters.

tethered radiometer while the ship was on station. The concentration of chlorophyll *a* [chl *a*] (mg m^{-3}), corrected for phaeopigment, was determined fluorometrically [*Strickland and Parsons*, 1972] on triplicate subsamples collected on GF/F filters, using a Turner Designs 10-005 R fluorometer (Sunnyvale, California) calibrated with chlorophyll *a* from Sigma-Aldrich.

[13] During transects of the eddy, bucket samples were also analyzed for a fluorescence-based measure of the maximum photosynthetic quantum yield of photosystem II, *Fv/Fm*, (dimensionless) using the photosynthetic inhibitor DCMU (3′-(3,3-dichlorophenyl)-1′,1′-dimethyl urea) [*Samuelsson and Öquist*, 1977; *Parkhill et al.*, 2001]. The samples were dark adapted for at least 30 min and triplicate subsamples were analyzed within an hour from sampling using a Turner Designs fluorometer (10-005 R). Fluorescence, corrected for a filtered seawater blank [*Cullen and Davis*, 2003] was measured before and 30 s after the addition of 50 μl of 3 mM DCMU in ethanol, following the protocol of *Parkhill et al.* [2001].

2.3. Initial Quality Control of Observations From the Drifters

[14] Records with time reversal (i.e., errors in ARGOS transmission) were eliminated from the analysis. Then, all exact repeats of optical or location data were removed. Finally, records with anomalous battery voltage were deleted. Only the optical records of the two drifters outside the eddy show signs of biofouling after 100 days according to the diagnostic used by *Abbott and Letelier* [1998], which is based on the ratio of upwelling radiances at 683 and 555 nm. Of all deployments, only data for the first 100 days are used in the presented analysis.

2.4. Spectrally and Daily Integrated Downwelling Irradiance

[15] The drifters recorded during daytime hours and transmitted the data approximately every hour. Irradiance in the photosynthetically available wave band, $E_d(\mathrm{PAR}, 0^+)$ (μmol quanta m^{-2} s^{-1}), defined as the integrated downwelling irradiance between 400 and 700 nm, was estimated from $E_d(490, 0^+)$ based on the following empirical relationship derived from regression analysis of hyperspectral TSRB data from the Bering Sea in 2000 and 2001 (r^2 = 0.9996, d.f. = 75, $p \ll 0.001$):

$$E_d(\mathrm{PAR}, 0^+) = 301\ \mathrm{nm} \cdot E_d(490, 0^+). \quad (1)$$

It is coincidental that incident solar spectral irradiance at 490 nm is nearly equal to the average for the PAR wave band. To estimate the daily integral of PAR (mol quanta m^{-2} d^{-1}) the data were interpolated linearly on a half-hour basis for the solar day and then integrated over daytime hours.

[16] Our analysis of fluorescence relies on estimates of scalar PAR just below the surface, $\mathring{E}(\mathrm{PAR}, 0^-)$ (μmol quanta m^{-2} s^{-1}), which requires estimation of transmission through the air-water interface ($\Re$, dimensionless) and the ratio of scalar to downwelling irradiance near the surface (dimensionless). Here we assume typical values of 0.97 for $\Re$, consistent with 3% surface reflection [*Kirk*, 1994], and 1.15 for $\mathring{E}(\mathrm{PAR}, 0^-)/E_d(\mathrm{PAR}, 0^-)$ [e.g., *Jerome et al.*, 1988], appreciating that more sophisticated estimates could be generated without significantly influencing our analyses of fluorescence versus irradiance:

$$\mathring{E}(\mathrm{PAR}, 0^-) = E_d(\mathrm{PAR}, 0^+) \cdot \Re \cdot \frac{\mathring{E}(\mathrm{PAR}, 0^-)}{E_d(\mathrm{PAR}, 0^-)} = 1.12 \cdot E_d(\mathrm{PAR}, 0^+). \quad (2)$$

2.5. Describing Properties of the Eddy

[17] The rotation period of the eddy was estimated from the positions of drifters eddy 1 and eddy 2 over time. The latitude and longitude data from the drifter time series were linearly interpolated to ensure equal spacing in time and were filtered twice (forward and backward) with a high-pass second-order Butterworth filter (cutoff frequency 21 days) [*Parks and Burrus*, 1987] to remove the eddy translation signal. The resultant time series were divided into overlapping 8-day segments with 4-day overlap and a sinusoidal model was fit to each segment using a Gauss-Newton least squares nonlinear curve fit:

$$x = r \cdot \sin(\omega t + \phi), \quad (3)$$

where x is the location of the drifter (evaluated for both north-south and east-west directions) and t is the time in decimal days. The fitted parameters r, ω, and ϕ are estimates of the radius of the trajectory, the rotation rate of the drifter, and the phase. Assuming negligible net slippage of the drifter, the parameter ω is also an estimator of the rotation rate of the eddy, so that $\omega = 2\pi/\tau_{\mathrm{rot}}$, where τ_{rot} is the period of a full rotation (days).

[18] To classify the eddy and provide insight on its dynamics, its Richardson (*Ri*) and Rossby (*Ro*) numbers were calculated as follows [*Gill*, 1982; *Knauss*, 1996]:

$$Ri = \frac{N^2}{\left(\frac{\partial u}{\partial z}\right)^2} \quad (4)$$

$$Ro = \frac{U}{fL}, \quad (5)$$

where N is the Brunt-Väisälä frequency (s^{-1}), $\partial u/\partial z$ is the gradient of horizontal velocities with depth (s^{-1}), U is the mean rim velocity (m s^{-1}), f is the Coriolis parameter (s^{-1}), and L is a characteristic length scale, here the radius of the eddy (m). The Brunt-Väisälä frequency was estimated from CTD data of one eddy transect of 11 stations taken on 23–24 June (Figure 2), where $N^2 = -(g/\rho_o)(\partial\rho/\partial z)$ and the reference density, ρ_o = 1028.8 kg m^{-3}. The CTD data have a depth resolution of 1 m and the spacing between stations is about 15 km along the transect. To increase resolution in this direction, the data were interpolated using a smoothing spline [*Chen and Mangasarian*, 1996], with the smoothing parameter P set to 0.999 based on visual criteria. The resolution of sampling for the calculated spline was set to ~2 km along the transect. The shear $\partial u/\partial z$ was estimated with the thermal wind equation [*Gill*, 1982] and CTD data from the same transect; in turn, the velocity in the rim region U was estimated to be 0.2–0.5 m s^{-1} and the

length scale L was estimated at 40–60 km. The Coriolis parameter was taken as 1.2×10^{-4} s^{-1} for all calculations.

2.6. Describing Variability in Fluorescence Emission

[19] Fluorescence emission, F (μmol quanta m^{-3} s^{-1}), is the product of absorbed irradiance and the quantum yield of fluorescence, with a correction for intracellular reabsorption of emitted photons [cf. *Babin et al.*, 1996; *Morrison*, 2003; *Huot et al.*, 2005]:

$$F = \overset{\circ}{E}(\mathrm{PAR}) \cdot \overline{a}_{\varphi} \cdot \phi_f \cdot Q_a^*, \tag{6}$$

where $\overset{\circ}{E}$(PAR) is scalar PAR irradiance (μmol quanta m^{-2} s^{-1}), $\overline{a}_{\varphi}$ (m^{-1}) is the absorption coefficient for phytoplankton, spectrally weighted for in situ irradiance over PAR [e.g., *Babin et al.*, 1996], ϕ_f is the quantum yield of fluorescence (mol photons emitted · (mol photons absorbed)$^{-1}$), and Q_a^* is a dimensionless factor representing the emitted fluorescence that is not reabsorbed within the cell.

[20] To examine the variation of fluorescence with irradiance, independent of changes in phytoplankton biomass (hence absorption), fluorescence can be normalized as

$$F^{\mathrm{abs}} = \frac{F}{\overline{a}_{\varphi} \cdot Q_a^*} = \overset{\circ}{E}(\mathrm{PAR}) \cdot \phi_f, \tag{7}$$

and F^{abs} (μmol quanta m^{-2} s^{-1}) can be described as a function of irradiance, much as others have done by analyzing the Sun-induced fluorescence signal normalized to chlorophyll [*Cullen et al.*, 1997; *Letelier et al.*, 1997; *Laney et al.*, 2005]. Note that F^{abs} normalized to $\overset{\circ}{E}$(PAR) is a direct estimate of quantum yield. Assumptions must be made, and corrections applied, to relate our observations of downwelling irradiance and upwelling radiance in the Bering Sea to fluorescence emission and its quantum yield. These are described below.

2.7. Relating Fluoresced Radiance at the Surface to Depth-Integrated Fluorescence Emission

[21] Our representation of the factors determining fluorescence emission, detected by the drifters as a near-surface fluorescence signal at 683 nm, is consistent with similar formulations [*Kiefer et al.*, 1989; *Babin et al.*, 1996; *Huot et al.*, 2005], with assumptions and simplifications that are described in following sections. Essentially, we integrate equation (6) with respect to depth:

$$L_{uf}(683) = \frac{1}{4\pi} \cdot \frac{1}{C_f} \cdot \overset{\circ}{E}(\mathrm{PAR}, 0^-) \cdot [\mathrm{chl}\,a] \cdot \overline{a}_{\varphi}^* \cdot \phi_f \cdot Q_a^* \cdot \frac{1}{\overline{K}_{\mathrm{abs}} + \kappa_f}. \tag{8}$$

The signal is upwelled fluoresced radiance at 683 nm, $L_{uf}(683)$ (μmol quanta m^{-2} s^{-1} nm^{-1} sr^{-1}). The first two terms on the right-hand side of the above equation relate volume emission of fluorescence over all emission wavelengths (μmol quanta m^{-3} s^{-1}) to upwelling fluoresced radiance at 683 nm: division by 4π sr reflects the assumption of isotropic emission, and division by C_f = 26.6 nm converts the emission over the whole fluorescence band to that at 683 nm, assuming a Gaussian distribution for the fluorescence emission centered at 683 nm with 25 nm width at half-maximum [*Gordon*, 1979; *Huot et al.*, 2005]. $\overset{\circ}{E}$(PAR, 0^-), the concentration of chlorophyll a ([chl a], mg chl a m^{-3}), and $\overline{a}_{\varphi}^*$ [m^2 (mg chl a)$^{-1}$], the specific absorption coefficient of the phytoplankton, weighted spectrally for the in situ irradiance spectrum [*Babin et al.*, 1996]. The final term in equation (8) accounts for the integration of volume emission with respect to depth [e.g., *Kiefer et al.*, 1989; *Babin et al.*, 1996]: $\overline{K}_{\mathrm{abs}}$ (m^{-1}) is the depth-averaged attenuation coefficient for absorbed radiation, and κ_f (m^{-1}) is the attenuation coefficient for upwelling radiance at 683 nm (both described below). Chlorophyll concentration and optical properties are assumed to be uniform in the upper few meters, where most of the water-leaving signal originates, and variations of ϕ_f with depth are neglected [*Babin et al.*, 1996; *Huot et al.*, 2005]. The dimensionless reabsorption factor, Q_a^* [*Babin et al.*, 1996], is set to 1.0, consistent with the small cells assumed to dominate during the study (see section 2.7.3), for which reabsorption is insignificant [cf. *Huot et al.*, 2005]. However, the influence of Q_a^* is considered in our sensitivity analysis.

2.7.1. Surface Chlorophyll *a* Concentrations From Ocean Color

[22] Optically based estimates of [chl a], chl$_{rs}$ (mg chl a m^{-3}), were obtained from the drifter data using the functional form of the SeaWiFS algorithm OC2 [*O'Reilly et al.*, 1998], parameterized with 1997 data from the OCP-100 and discrete chlorophyll samples taken simultaneously from bucket samples (see Figure 3a):

$$\mathrm{chl}_{rs} = 0.0044 + 10^{\left(0.3917 - 1.3000 \cdot \log_{10}\left(\frac{R(490)}{R(555)}\right) - 2.2884 \cdot \left(\log_{10}\left(\frac{R(490)}{R(555)}\right)\right)^2 - 6.9496 \cdot \left(\log_{10}\left(\frac{R(490)}{R(555)}\right)\right)^3\right)}, \tag{9}$$

where $R(\lambda)$ is the radiance reflectance at a given wavelength ($L_u(\lambda)/E_d(\lambda, 0^+)$, sr^{-1}; $L_u(\lambda)$ measured at 20 cm). Recognizing its ties to the Bio-Optical Algorithm MiniWorkshop (SeaBAM) algorithm, our implementation for the Bering Sea will be referred to as BSBAM; best-fit parameters were determined using a nonlinear least squares analysis implemented in MATLAB (nlinfit), with an r^2 of 0.94 (d.f. = 50, $p \ll 0.001$). Since the drifters only record downwelling irradiance at 490 nm, $E_d(555, 0^+)$ was estimated as a function of $E_d(490, 0^+)$ according to a relationship developed using OCP-100 data from the Bering Sea cruise in 1997: linear regression of $E_d(555, 0^+)$ on $E_d(490, 0^+)$ reveals that the y-intercept is insignificant and the regression was therefore forced through the origin to yield the relationship, $E_d(555, 0^+) = 1.032 \cdot E_d(490, 0^+)$ (r^2 = 0.9995, d.f. = 50, $p \ll 0.001$).

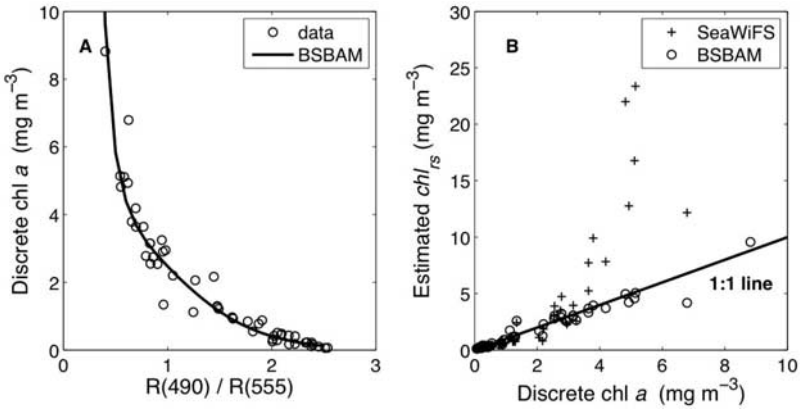

Figure 3. (a) Locally parameterized OC2-type ocean color algorithm for chl *a* estimation in the Bering Sea (BSBAM), relating the concentration of chlorophyll to the ratio of reflectance at 490 nm to that at 555 nm (equation (9)). (b) Chl_{rs} estimated using the BSBAM algorithm (circles) and the global parameter set of the Sea-viewing Wide Field-of-view Sensor (SeaWiFS) OC2 algorithm (crosses).

[23] Figure 3b shows a comparison of chl_{rs} estimates from BSBAM and the global SeaWiFS algorithm OC2 [*O'Reilly et al.*, 1998]. Prevailing high chromophoric dissolved organic matter (CDOM) concentrations in the Bering Sea introduce a bias when global parameters for the algorithm are used. Clearly, the local parameterization corrects for this bias and increases the reliability of the estimate.

2.7.2. Correction for Backscattered Solar Radiation

[24] In order to estimate upwelled fluorescence, $L_{uf}(683)$ in equation (8), the measured radiance, $L_u(683)$, must be corrected for other sources of red photons, Raman scatter and backscattered sunlight at 683 nm, $L_{ub}(683)$. For Bering Sea waters of relatively high concentrations of CDOM and chlorophyll, we ignore Raman scatter [see *Huot et al.*, 2007]:

$$L_{uf}(683) = L_u(683) - L_{ub}(683). \quad (10)$$

When observations in only a few wave bands are available, the correction for solar backscatter is commonly determined from a linear baseline between measurements of $L_u(\lambda)$ on either side of the red fluorescence band [*Abbott and Letelier*, 1999; *Huot et al.*, 2005]. However, the longest wavelength detected by the optical drifters was 683 nm, so $L_{ub}(683)$ was estimated by using linear regressions to examine the relationships between (1) variables that could be retrieved from the multispectral optical drifters (e.g., $L_u(670)$, employed by *Letelier et al.* [1997], or alternates such as $L_u(555)$) and (2) $L_{ub}(683)$, estimated from a linear baseline between $L_u(654)$ and $L_u(723)$, all retrieved from highly resolved spectra collected with a hyperspectral radiometer buoy during $n = 69$ deployments in the Bering Sea during 2000 and 2001 (section 2.1) when no coccolithophores were present (see below).

[25] It was found that the upwelling radiance at 555 nm, multiplied by the factor 0.128, was the best estimator of the linear baseline between $L_u(654)$ and $L_u(723)$, which provided our definition of $L_{ub}(683)$. Our operational version of equation (10) is thus $L_{uf}(683) = L_u(683) - (L_u(555) \cdot 0.128)$; $r^2 = 0.98$, d.f. = 68, $p \ll 0.001$ (Figure 4). The use of $L_u(555)$ for the correction is unconventional, but as shown in Figure 4, it is better than a correction based on $L_u(670)$, probably because $L_u(555)$ is unaffected by fluorescence. This is not the case for $L_u(670)$, as phytoplankton fluoresce at wavelengths as low as 660 nm [*Gordon*, 1979; *Culver and Perry*, 1997]. Also, because upwelling radiance at 555 nm is largely unaffected by the presence of chlorophyll *a*, its variation is dominated by changes in backscattering coefficients, and backscatter is responsible for $L_{ub}(683)$. An exception is expected when $L_u(555)$ is affected by the presence of coccolithophores because of their high scattering efficiency and relatively flat spectral dependence of backscatter [*Balch et al.*, 1996]. For this reason, deployments where the presence of coccolithophores was suspected, as indicated by $R(555) > 0.01$ sr^{-1}, were excluded from the 2000–2001 data set used to derive this backscatter correction. Note that the 1997 drifter data were screened for the presence of coccolithophores according to the above criterion but the threshold reflectance was not exceeded.

2.7.3. Estimation of the Mean Specific Absorption Coefficient for Phytoplankton

[26] It has been shown that the chlorophyll *a* specific absorption coefficient at 512 nm, $a_\varphi^*(512)$ (m^2 [mg chl *a*]$^{-1}$), is nearly equal to the mean chlorophyll specific absorption coefficient for a wide range of phytoplankton absorption spectra [*Bricaud et al.*, 1995; *Ciotti et al.*, 2002]; it also serves as a proxy for $\overline{a}_\varphi^*$, the specific absorption coefficient weighted for the surface irradiance spectrum, as is appropriate for our application [*Huot et al.*, 2005]. We thus use $a_\varphi^*(512)$ to estimate $\overline{a}_\varphi^*$. Visual inspection of samples from shipboard measurements and inference from HPLC pigment analysis showed that a bloom encountered by the drifters at the beginning of deployment consisted mainly of *Phaeocystis* colonies. *Ciotti et al.* [2002] assigned samples from the same bloom to the ultraplankton size class according to absorption characteristics. Later in the summer we expected smaller cells, so in the absence of direct observations of the changes in absorption with [chl *a*], we assumed a fixed $a_\varphi^*(512) = 0.0131$ m^2 mg chl^{-1} as reported

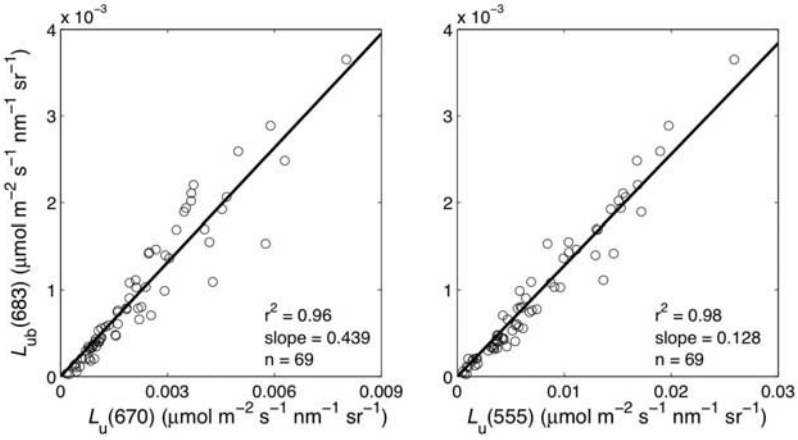

Figure 4. Comparison of relationships between solar backscatter at 683 nm and upwelling radiances at 670 and 555 nm as measured with a hyperspectral instrument in the Bering Sea in 2000 and 2001. Solar backscatter at 683 nm has been estimated from a baseline applied to the hyperspectral data (see section 2.7.2 for details). The line in both panels represents the slope of the regression forced through the origin; the slope in the right-hand panel is used for the backscatter correction of the drifter data.

by *Ciotti et al.* [2002] for average nanoplankton. For comparison, we also analyzed the data of drifter eddy 1 employing the empirical formulation by *Bricaud et al.* [1995], where $a^*_\varphi(512)$ decreases as a function of chl *a*, $a^*_\varphi(512) = 0.0171 \cdot \mathrm{chl}_{rs}{}^{-0.249}$, consistent with larger cells in higher [chl *a*] water [*Ciotti et al.*, 1999].

2.7.4. Attenuation Coefficients for Absorbed Radiation and Emitted Photons

[27] Using a simplification of the approach described by *Huot et al.* [2005], we estimated the mean attenuation coefficient for photosynthetically available radiation absorbed by phytoplankton, $\overline{K}_{\mathrm{abs}}$, using an empirical formulation based on data from the Bering Sea cruise in 1997. Measurements from the profiling radiometer were used to derive attenuation coefficients, $K_d(\lambda)$, at 10 discrete wavelengths (λ = 338, 412, 443, 490, 510, 531, 555, 670, 683, and 701 nm, omitting data from three additional channels that all measured below 400 nm) by performing a linear fit to the log transformed data from 1.5 to 5 m. The estimated attenuation coefficients are thus representative of the surface mixed layer where more than 90% of the fluorescence measured at the surface originates [*Topliss*, 1985; *Babin et al.*, 1996]. The discrete estimates of $K_d(\lambda)$ were linearly interpolated with unit spacing for the 400–700 nm domain. Using an average downwelling irradiance spectrum for the Bering Sea and the average specific absorption spectrum for nanoplankton as reported by *Ciotti et al.* [2002], the absorbed radiation per unit volume at a given depth, $A_{\mathrm{abs}}(z)$ (μmol quanta m^{-3} s^{-1}), was calculated as follows [*Huot et al.*, 2005]:

$$A_{\mathrm{abs}}(z) = \mathrm{chl}_{rs} \cdot \int_{400}^{700} a^*_\varphi(\lambda) \cdot \overset{\circ}{E}(\lambda, 0^-) \cdot e^{-K_d(\lambda)\cdot z} \cdot d\lambda. \qquad (11)$$

From the estimates of $A_{\mathrm{abs}}(z)$ for discrete depths with a spacing of 10 cm, the depth of 10% $A_{\mathrm{abs}}(0^-)$ for each station was determined. For each profile, a log regression on $A_{\mathrm{abs}}(z)/A_{\mathrm{abs}}(0^-)$ versus depth from the surface to 10% $A_{\mathrm{abs}}(0^-)$ was then performed to estimate $\overline{K}_{\mathrm{abs}}$. The resulting values for $\overline{K}_{\mathrm{abs}}$ were then regressed against corresponding chl_{rs} estimates from the OCP-100, yielding the following relationship (r^2 = 0.95, d.f. = 39, $p \ll 0.001$):

$$\overline{K}_{\mathrm{abs}} = 0.077 + 0.046 \cdot \mathrm{chl}_{rs}. \qquad (12)$$

This local parameterization should differ from calculations based on global data sets because of the prevailing high CDOM concentrations in the Bering Sea (see chl_{rs} estimation; section 2.7.1).

[28] Attenuation of upwelling fluoresced radiance is dominated by absorption [*Kiefer et al.*, 1989; *Maritorena et al.*, 2000], so the attenuation coefficient κ_f was assumed to be

$$\kappa_f = a_w(683) + a_\varphi(683), \qquad (13)$$

where the absorption by water, $a_w(683)$, is 0.478 m^{-1}, taken from *Pope and Fry* [1997] and absorption by phytoplankton, $a_\varphi(683)$, is estimated as

$$a_\varphi(683) = a^*_\varphi(683) \cdot \mathrm{chl}_{rs}, \qquad (14)$$

with $a^*_\varphi(683)$ = 0.0126 m^2 mg chl^{-1} as reported for average nanoplankton in *Ciotti et al.* [2002]. Expected variation of $a^*_\varphi(683)$ with [chl *a*] [*Bricaud et al.*, 1995] would have little influence on the estimation of κ_f because $a_w(683)$ dominates in equation (13).

2.7.5. Quality Control for Optical Estimates of Chlorophyll and Fluorescence

[29] For estimates of chlorophyll based on measurements of upwelling radiance in the blue and green wave bands (section 2.7.1), all records from the drifters with downwelling irradiance, $E_d(490, 0^+)$, $\leq$0.2 μmol quanta m^{-2} s^{-1} nm^{-1} (corresponding to about 4% of midday clear-sky irradiance at this latitude) were discarded because of small

reflectance signals at the relevant wavelengths, 490 nm and 555 nm, associated with weak sunlight. The quality control routine also removed all records for $L_u(490)$ and $L_u(555)$ whose standard deviation as transmitted by the drifter was greater than 20% of the mean. Finally, all records with negative calculated chlorophyll concentration were discarded. The application of the full quality control routine resulted in about 60% of the point estimates of chl_{rs} being removed, mostly corresponding to records from low irradiance.

[30] These signal-based criteria were not applied in the analysis of fluorescence at 683 nm (section 2.7.2) because the upwelling radiance sensor for 683 nm had enhanced sensitivity and thus could discern light-dependent variability in fluorescence emission even when the estimation of chlorophyll was compromised. Consequently, the number of records of fluorescence exceeded that for chlorophyll by a factor of 1.7. Our analyses of fluorescence yield as a function of irradiance require estimates of chlorophyll for each observation, so the mismatch in numbers of observations was addressed by using 2-day averages of estimated chlorophyll concentration from the drifters (see section 2.8).

2.8. Estimating Fluorescence Normalized to Absorption

[31] To describe the variability of near-surface fluorescence yield as a function of irradiance, the terms in equation (8) can be rearranged to be consistent with the definition of F^{abs} in equation (7):

$$F^{\mathrm{abs}} = \mathring{E}(\mathrm{PAR}, 0^-) \cdot \phi_f = \frac{L_{uf}(683) \cdot 4\pi \cdot C_f}{[\mathrm{chl}\,a] \cdot \overline{a}^*_\varphi \cdot Q^*_a} \cdot \left[\overline{K}_{\mathrm{abs}} + \kappa_f\right]. \quad (15)$$

As shown in preceding sections, variables in the right-hand side of equation (15) can be described as functions of remotely sensed optical data, yielding ocean color–based estimates of fluorescence normalized to absorption, F^{abs}_{rs} (μmol quanta m^{-2} s^{-1}). The general form is

$$F^{\mathrm{abs}}_{rs} = \frac{(L_u(683) - L_{ub}(683)) \cdot 4\pi \cdot C_f}{\mathrm{chl}_{rs} \cdot \overline{a}^*_\varphi(\mathrm{chl}_{rs}) \cdot Q^*_a(\mathrm{chl}_{rs})} \cdot \left[\overline{K}_{\mathrm{abs}}(\mathrm{chl}_{rs}) + \kappa_f(\mathrm{chl}_{rs})\right], \quad (16)$$

where the dependencies of variables on optically derived chlorophyll concentration (chl_{rs}) reflect both the contribution of phytoplankton to the attenuation of light ($\overline{K}_{\mathrm{abs}}$ and κ_f) and the general relationships between optical properties of phytoplankton (a^*_φ and Q^*_a) and chl_{rs} as a proxy for trophic status [e.g., *Bricaud et al.*, 1995; *Ciotti et al.*, 1999].

[32] Parameterization of phytoplankton absorption coefficients as a function of chl_{rs} would be uncertain, so for our initial analysis we simplify equation (16) by assuming that $\overline{a}^*_\varphi = 0.0131$ m^2 mg chl^{-1} and $Q^*_a = 1.0$ as described above, and substituting our derived functions for $\overline{K}_{\mathrm{abs}}$ and κ_f:

$$F^{\mathrm{abs}}_{rs} = \frac{(L_u(683) - (L_u(555) \cdot 0.128)) \cdot 4\pi \cdot 26.6}{\mathrm{chl}_{rs} \cdot 0.0131 \cdot 1.0} \cdot [(0.077 + 0.046 \cdot \mathrm{chl}_{rs}) + (0.478 + 0.0126 \cdot \mathrm{chl}_{rs})]. \quad (17)$$

This equation further simplifies to $F^{\mathrm{abs}}_{rs} = (\mathrm{FLH}/\mathrm{chl}_{rs}) \cdot (14{,}162 + 1495 \cdot \mathrm{chl}_{rs})$. We analyze F^{abs}_{rs} as a function of surface irradiance, much as photosynthesis versus irradiance is studied. In turn, $F^{\mathrm{abs}}_{rs}/\mathring{E}(\mathrm{PAR}, 0^-)$ is an estimate of the quantum yield of fluorescence, ϕ_f (equation (7)); we examine its behavior as well.

[33] Time series data from the drifters were divided into overlapping 2-day segments and for each segment, F^{abs}_{rs} was plotted as a function of $\mathring{E}(\mathrm{PAR}, 0^-)$. Initial analysis indicated that the relationship was nonlinear, i.e., the slope decreased at higher irradiance [cf. *Laney et al.*, 2005], and that a small number of points departed strongly from a smooth relationship between fluorescence and irradiance.

[34] To address outliers, each set of observations was fitted to a second-order polynomial using a robust regression method [*Huber*, 1981] provided by the rlm algorithm [*Venables and Ripley*, 1994] of the R statistical language [*R Development Core Team*, 2007]. The deviations between observed and regressed fluorescence values were tabulated and then normalized to a Z value by subtracting the mean and dividing by the standard deviation. Observations for which Z exceeded a threshold Z_C were then flagged as outliers. The value $Z_C = 2.5$, which excludes observations >2.5 standard deviations from the regression line, was found to match well with visual outlier selection for one set of observations (eddy 1) and was then applied to the entire data set. As a result, about 3 percent of observations were classified as outliers.

[35] Parameter values were then estimated for the following model describing a relationship between F^{abs}_{rs} and $\mathring{E}(\mathrm{PAR}, 0^-)$:

$$F^{\mathrm{abs}}_{rs} = F^{\mathrm{abs}}_{\max} \cdot \left\{1 - \exp\left[-\left(\frac{\alpha^{\mathrm{abs}}_F \cdot \mathring{E}(\mathrm{PAR}, 0^-)}{F^{\mathrm{abs}}_{\max}}\right)\right]\right\}, \quad (18)$$

where $F^{\mathrm{abs}}_{\max}$ (μmol quanta m^{-2} s^{-1}) is the maximum fluorescence normalized to absorption in high light and α^{abs}_F (dimensionless) is the initial slope of the F^{abs}_{rs} versus irradiance relationship. Representative examples are presented in Figure 5. On average, 18 estimates of fluorescence were available per segment; for many of those in low light, estimates of chl_{rs} were unavailable due to sensitivity problems (section 2.7.5), so the 2-day average was used for all estimates of chl_{rs} in an interval, assuming that most of the short-term, light-dependent variability in F^{abs}_{rs} is attributable to fluorescence emission, and not confounding changes in the absorption of light by phytoplankton. Estimation of $F^{\mathrm{abs}}_{\max}$ and α^{abs}_F, with their 95% confidence limits, was carried out using a least squares nonlinear curve fit implemented in MATLAB (nlinfit). To eliminate nonconvergent or particularly uncertain results we only accepted estimates of α^{abs}_F and $F^{\mathrm{abs}}_{\max}$ from fits whose 95% confidence intervals (ci) satisfied the following criteria: $ci < 2 \cdot \mathrm{median}\,(\alpha^{\mathrm{abs}}_F)$ and $ci < 2 \cdot \mathrm{median}\,(F^{\mathrm{abs}}_{\max})$, respectively. In addition, F^{abs}_{1500}, normalized fluorescence at 1500 μmol quanta m^{-2} s^{-1}, was also estimated, along with confidence limits. The corresponding quantum yield of fluorescence, $\phi_f(1500)$, is $F^{\mathrm{abs}}_{1500}/\mathring{E}(\mathrm{PAR}, 0^-)$; see equation (15).

[36] Appreciating that florescence may not reach an asymptotic maximum at high irradiance, we also fit the

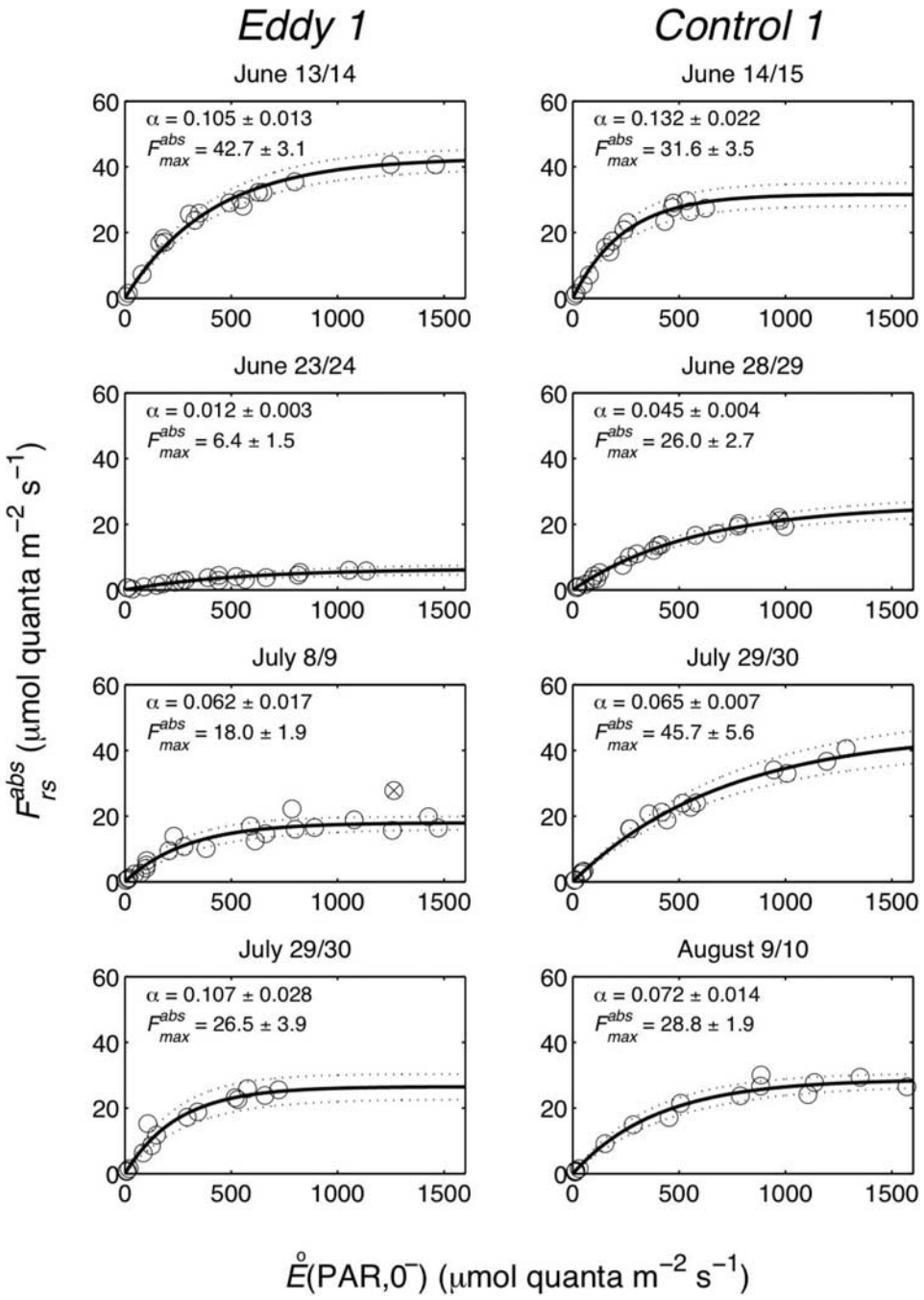

Figure 5. Exemplary fluorescence-irradiance curve fits (±95% confidence intervals on the fits and parameters) for the drifter data, taken from the records of drifters eddy 1 (left) and control 1 (right). The data were fit to equation (18) in 2-day time intervals. Estimated fluorescence normalized to absorption, F^{abs}_{rs}, is plotted versus photosynthetically available radiation just below the surface. Circles represent drifter data, and crosses indicate outliers that were omitted from the curve fits.

same data to the bilinear model of *Laney et al.* [2005] using the lsqcurvefit routine in MATLAB:

$$F_{rs}^{\mathrm{abs}} = \left(\beta_1 \cdot \overset{\circ}{E}(\mathrm{PAR}, 0^-) \cdot \left[\overset{\circ}{E}(\mathrm{PAR}, 0^-) < E_b\right]\right) + \left(\left((\beta_1 \cdot E_b) + \left(\beta_2 \cdot \left(\overset{\circ}{E}(\mathrm{PAR}, 0^-) - E_b\right)\right)\right) \cdot \left[\overset{\circ}{E}(\mathrm{PAR}, 0^-) \geq E_b\right]\right) \quad (19)$$

where β_1 and β_2 are initial and final slopes (dimensionless), E_b is the break point where the two lines meet (μmol quanta m^{-2} s^{-1}) and the terms in brackets are Boolean operators defining the ranges of $\overset{\circ}{E}(\mathrm{PAR}, 0^-)$ for which each line applies. Judging by probabilities from *F*-tests calculated with the anova algorithm in R, the three-parameter bilinear model frequently fit the data better than the two-parameter exponential model. However, the two-parameter exponential model nearly always converged whereas the bilinear model failed to produce results for about one third of the curves. Although the bilinear model generally indicated that normalized fluorescence continued to increase in high light, estimates of both the initial slopes (α_F^{abs} and β_1) and F_{1500}^{abs} for the two models were highly correlated ($r \geq 0.90$ and $p \ll 0.001$ except for one case (F_{1500}^{abs}, control 1), where $r = 0.78$, but still $p \ll 0.001$). Because both models yielded similar estimates of fluorescence yield and one generated usable curve fits more frequently, we used the exponential model for our analysis of variability of fluorescence yield in low and high light during this study.

3. Results

3.1. Sea Surface Temperature, Incident Irradiance, Chlorophyll *a*, and Photochemical Efficiency

[37] All drifters recorded a sea surface temperature (SST) trend consistent with seasonal warming of the surface waters, interrupted by transient increases that may have been due to stratification, and sudden coolings, presumably during sporadic mixing events (Figure 6a). Integrated daily PAR (Figure 6b) shows the influence of varying degrees of the Bering Sea's chronic cloudiness on the gradual decrease of clear-sky solar radiation after the summer solstice. SST and daily PAR were generally coherent across all four drifters.

[38] At the beginning of the record, all drifters encountered the final stages of a phytoplankton bloom, apparent in the high retrieved chlorophyll concentrations (Figure 6c). This is reflected in direct determinations of [chl *a*] from transects across the eddy near the end of the bloom on 11 June and on 23 June, after it had collapsed (Figure 7a). Measurements of photochemical efficiency, *Fv*/*Fm*, made on the same samples (Figure 7b), suggest that phytoplankton in the eddy were nutrient deficient just prior to the decline of the bloom: on 11 June mean *Fv*/*Fm* was 0.407 (s.d. = 0.096, $n = 4$). After the bloom had subsided, on 23 June, *Fv*/*Fm* across the eddy was 0.600 (s.d. = 0.044, $n = 5$), suggesting that the new community established after the bloom was subjected to less nutrient stress [cf. *Falkowski and Kolber*, 1995; *Parkhill et al.*, 2001]. These direct assessments of photochemical efficiency provide a rare opportunity to relate measurements of Sun-induced chlorophyll fluorescence yield to independent assessments of the physiological status of phytoplankton in natural surface waters.

[39] After the bloom and its collapse, chl_{rs} estimates from the four drifters varied somewhat independently of each other, with estimated chlorophyll concentration rising from a minimum of about 2 mg m^{-3} in late June to about 8 mg m^{-3} in late July or August, followed by a decline (Figure 6).

3.2. Description of the Eddy

[40] During the first 35 days of drifter observation, the eddy translated southwestward at about 0.05 m s^{-1} and stayed more or less in one location from mid-July until the end of observation (Figure 1). According to the shipboard observations during a transect on 23–24 June, the eddy had a diameter of 120–150 km and extended to a depth of ~1000 m (Figure 2). The Rossby number *Ro* is estimated as 0.03 to 0.1, given the range of estimates of eddy radius and velocity. This range of Rossby numbers indicates that the eddy's flow is in geostrophic balance, justifying the use of thermal wind calculations for large-scale Richardson number. This is born out by isopycnal deformation within the eddy, depressed by up to 100 m at the center. The gradient Richardson number *Ri* for the transect fails to achieve the critical value for vigorous mixing throughout the eddy, although one may expect enhanced mixing at locations of steep isopycnal slopes (such as where drifters eddy 1 and 2 were deployed) that thermal wind calculations suggest will have high shears, and at times of relatively high eddy rotation rates.

3.3. Rotation Period

[41] The records of drifters eddy 1 and eddy 2 were used to estimate the rotation period of the eddy (Figure 6f). At the beginning of observations by drifter eddy 1, the eddy took about 5 days for a full rotation. This time increased to 10 days for a few weeks, then decreased and increased again at the end of the record. Good agreement of drifter velocities with rotational velocities in the high-velocity region of the eddy as estimated from the CTD transect (thermal wind calculation; data not shown) suggests that drifter eddy 1 traveled in the high-velocity region of the eddy at the beginning of deployment and there is no indication that it left this region during the period of observation. By contrast, the drifter eddy 2 appeared to stay in the high-velocity region of the eddy only until mid-July (Figure 6f), and then moved to a slower trajectory farther out, but still within the rim region of the eddy, hence the higher estimates of rotation period after mid-July.

3.4. Fluorescence Yield Versus Irradiance

[42] As shown in the comparison of representative F_{rs}^{abs} versus irradiance curves (Figure 5) and the time series from the four drifters (Figures 6d and 6e), the normalized fluorescence-irradiance relationship shows substantial variability as a function of time. The parameter α_F^{abs}, which is an estimate of ϕ_f at low irradiance, varies by about 1 order of magnitude, comparable to the range observed by *Letelier et al.* [1997], who quantified the slope of $\mathrm{FLH}/\mathrm{chl}_{rs}$ versus $E_d(490)$ as their only estimate of ϕ_f. There is also considerable variation in F_{1500}^{abs} and thus $\phi_f(1500)$, almost a factor

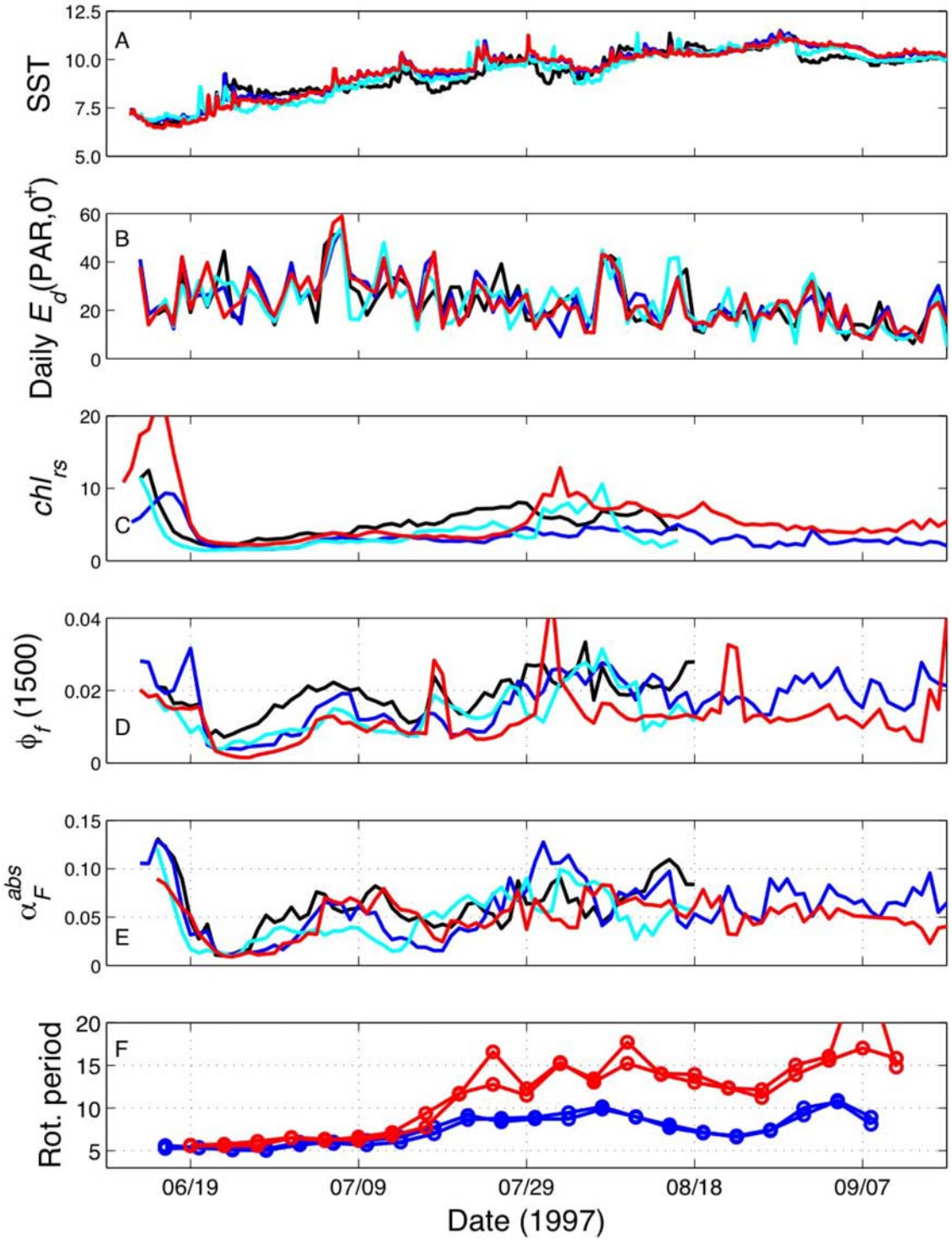

Figure 6. Records from the four drifters (blue, eddy 1; red, eddy 2; black, control 1; cyan, control 2): (a) sea surface temperature; (b) integrated daily E_d(PAR, 0^+) (mol quanta m^{-2} d^{-1}); (c) daily averaged chl_{rs} (mg m^{-3}); (d) ϕ_f(1500) (dimensionless), estimated from curve fits; (e) α_F^{abs} (dimensionless), estimated from curve fits; (f) rotation timescales of the eddy as derived from positions of the two drifters traveling in the eddy (curves of the same color show estimates from north-south versus east-west position).

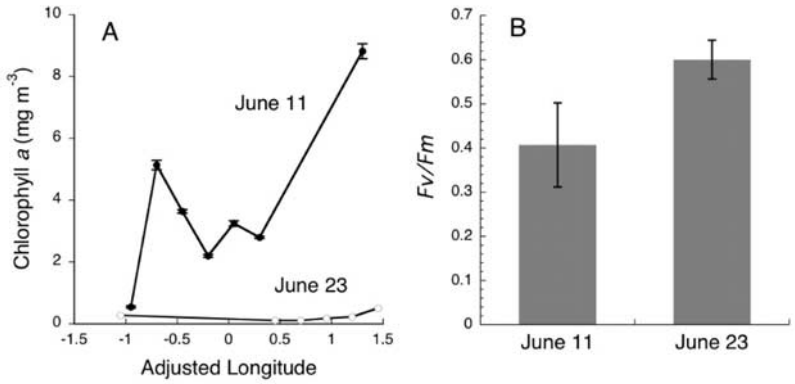

Figure 7. (a) Chlorophyll *a* (±SE, $n = 3$) measured on two transects through the eddy, with position represented as adjusted longitude, relative to the center. The transect on 11 June encountered the phytoplankton bloom, also recorded in the drifter data, just before its peak. The second transect (23 June) was taken after the decline of the bloom. (b) Measurements of photochemical efficiency (*Fv*/*Fm* ± s.d., $n = 4$ on 11 June and $n = 5$ on 23 June) (from J. P. Parkhill, unpublished data, 1997) suggest that phytoplankton were nutrient-stressed near the end of the bloom (low *Fv*/*Fm*) and that this stress relaxed after the bloom had crashed.

of 10. The confidence limits on α_F^{abs} and $\phi_f(1500)$ are generally small relative to temporal variability in the estimates (Figure 9), indicating that data from the drifters are sufficient to constrain our model describing the variability of Sun-induced fluorescence quantum yield in low and high light during the study.

4. Discussion

4.1. General Patterns

[43] The sea surface temperature records for all drifters were characterized by seasonal warming with significant meteorological scale variability; the SST and PAR records for all four drifters (Figures 6a and 6b) are in good agreement, indicating that they encountered similar conditions in terms of these large-scale physical variables. Chlorophyll concentrations estimated from drifter data did not fall below 2 mg m^{-3} during the 3-month observation period. The BSBAM algorithm performed well in low-chlorophyll regimes (Figure 3) and is customized for the high CDOM concentrations in the Bering Sea (section 2.7.1). We therefore assume that the relatively high chl_{rs} estimates are not an artifact, especially as the eastern Bering Sea is known to be a highly productive area during summer [*National Research Council*, 1996; *Springer et al.*, 1996], but it is possible that detritus left after the decline of the phytoplankton bloom added to the chl_{rs} estimates.

[44] Noteworthy variations in chl_{rs} include the initial bloom that declined shortly after deployment of the drifters, and fairly coherent, but not completely coincident blooms of about 2 weeks' duration in early August (Figure 6c). Fluorescence parameters were more variable: both α_F^{abs} and $\phi_f(1500)$ declined sharply along with the bloom (Figures 5, 6d, and 6e) and varied on a scale of days to weeks thereafter, in patterns that will be examined below.

4.2. Eddy Dynamics and Nutrient Input

[45] Drifter tracks (Figure 1) and density surfaces from a transect (Figure 2) show that the eddy encountered by two of the four drifters in this study was anticyclonic. The low value of the measured Rossby number indicates geostrophic conditions, and so the thermal wind relationship links vertical shears with horizontal density gradients. This suggests that Richardson numbers will be relatively low in the eddy rim region. Assuming a statistically uniform background shear, perhaps caused by internal waves, the expectation is thus that nutrient fluxes from deep waters up into the euphotic zone may be highest in the rim region.

[46] In addition to this mixing mechanism, it has been suggested that there is a secondary circulation in eddies that transports nutrients along isopycnals [*Yentsch and Phinney*, 1985; *Franks et al.*, 1986; *Lee and Williams*, 2000]. This yields an enhanced upward flux component where isopycnals are most sloped, i.e., at the rim of the eddy. Secondary circulation, submesoscale processes, and departures from geostrophic balance can also effect other cross-frontal fluxes [*Lévy et al.*, 2001; *Martin and Richards*, 2001], and several researchers have stressed the potential importance of such fluxes for eddies and meanders [e.g., *Yentsch and Phinney*, 1985; *Lohrenz et al.*, 1993; *Lee and Williams*, 2000], particularly in conjunction with a speedup of the mean flow [e.g., *Williams and Follows*, 2003]. Since two drifters in this study stayed in the rim region of the eddy for up to 3 months (i.e., 20–50 km away from the eddy's center), the optical properties observed may be influenced by nutrient fluxes associated with both shear instabilities and the secondary circulation. These mechanisms suggest increased nutrient fluxes with increasing rotation rates of the eddy, so it is feasible to interpret variations in the rotational velocity over time in terms of nutrient flux to the surface in the rim region of the eddy: a faster spinning eddy would be associated with increased nutrient flux.

[47] The combination of nutrient fluxes from the above-described processes in the rim region of an anticyclonic eddy may explain the high phytoplankton concentrations that have been observed by several authors [*Hitchcock et al.*, 1993; *Pérez et al.*, 2003]. In addition, sporadic submesoscale cross-frontal exchange as found in modeling studies by *Lévy et al.* [2001] may play a role in the supply of nutrients to the rim region of an anticyclonic eddy.

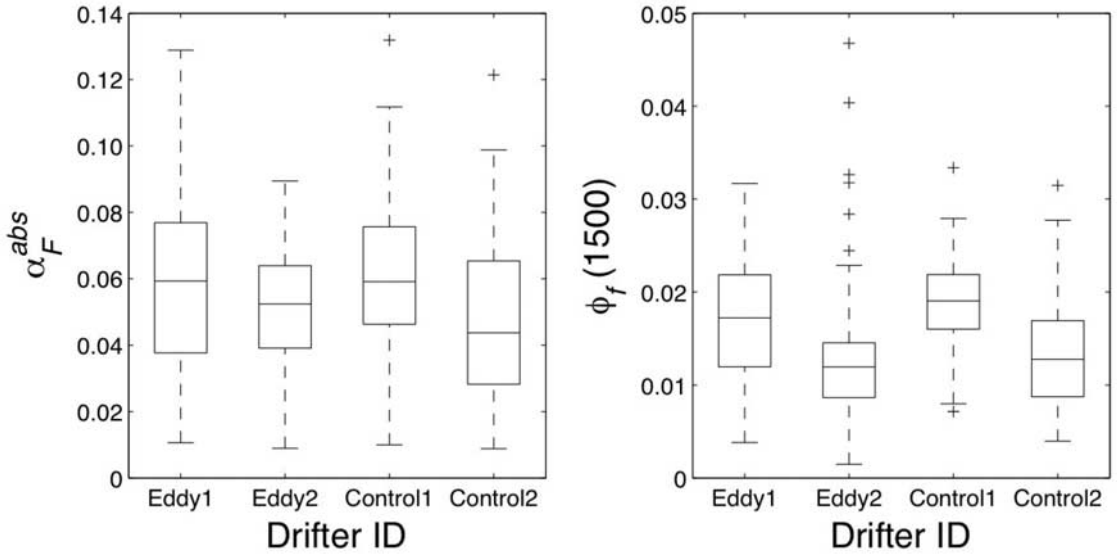

Figure 8. Variability in parameters of the F_{rs}^{abs} versus E relationship: (a) the initial slope, α_F^{abs} (dimensionless), and (b) the fluorescence quantum yield at 1500 μmol quanta m^{-2} s^{-1}, $\phi_f(1500)$ (dimensionless), observed by different drifters. The respective lines inside the boxes indicate the medians of the observed parameters, the boxes indicate the range from the first to the third quartile, the dashed lines connect to the highest and lowest points within 1.5 times the interquartile range from the median, and outliers are indicated by crosses.

4.3. Variability of the Fluorescence-Irradiance Relationship

[48] It has already been shown that the relationship between SICF and solar radiation at the sea surface varies significantly on the timescale of days and that a proxy of the quantum yield of fluorescence was correlated with nutrient flux, as inferred from a model of eddy dynamics [*Letelier et al.*, 1997]. We attempted to test this by employing a more detailed model that accounts for optical properties of the water column while retrieving the quantum yield of fluorescence directly [*Babin et al.*, 1996; *Huot et al.*, 2005], and by fitting the results to a function that includes both the initial slope of the fluorescence versus irradiance relationship and an estimate of fluorescence yield in high light relevant to satellite remote sensing under clear skies. As shown below, the improved analysis reinforces the conclusions of earlier studies, that high fluorescence yields were associated with nutrient stress, but leads to a new explanation for the mechanistic basis for the observed variability.

4.3.1. Scale of Variability and Sensitivity to Assumptions

[49] Examples of F^{abs} versus E curves (Figure 5) and records of the variability in α_F^{abs} and $\phi_f(1500)$ (Figures 6 and 8) show that the initial slope of the relationship varied by almost a factor of 10 over periods as short as a few days; the magnitude and timescale of variability is very close to that observed by *Letelier et al.* [1997], who quantified the FLH/chl versus E slope to estimate an apparent quantum yield similar to α_F^{abs}, whereas *Abbott et al.* [2001] observed only two- to threefold variability during deployments of drifters in Antarctic Polar Front meanders. Variability of the quantum yield of fluorescence at 1500 μmol m^{-2} s^{-1} is similar (Figure 8); the range, from less than 0.01 to 0.03 for most of the points, is consistent with, but on the high end, of the estimates from remote sensing generated by *Huot et al.* [2005], which had a median of 0.012. Their estimates were, in turn, marginally higher than reports from comparable studies [*Ostrowska et al.*, 1997; *Maritorena et al.*, 2000; *Morrison*, 2003].

[50] As discussed below, more than fivefold changes in fluorescence yield over the span of a few days are difficult to explain with commonly invoked models of the effects of nutrients on photosynthesis and fluorescence; it is therefore important to determine whether biases in our analyses, particularly in the estimation of F_{rs}^{abs} (equation (16)), could have accentuated the inferred variability or otherwise confounded our results. Given commonly used descriptions of how optical properties vary with [chl a] [cf. *Bricaud et al.*, 1995; *Babin et al.*, 1996], *Huot et al.* [2005] calculated that the cumulative effect of the correction term, $[\overline{K}_{\text{abs}}(\text{chl}_{rs}) + \kappa_f(\text{chl}_{rs})]/[\overline{a}_{\varphi}^{*}(\text{chl}_{rs}) \cdot Q_a^{*}(\text{chl}_{rs})]$ (parameterized in a slightly different way), on the estimation of what we call F_{rs}^{abs} is about a factor of 10 over the range from 1.0 to about 30 mg m^{-3} chl_{rs}, and fourfold over the range, 1.0 to 10 mg m^{-3}. If all components of the correction term are assumed to be constant (as is done implicitly by using FLH/chl as a measure of fluorescence normalized to absorption), the correction term and thus F_{rs}^{abs} will be underestimated roughly in proportion to the concentration of chlorophyll. It is noteworthy that some of our highest fluorescence yields were observed on 12–13 June, when both estimated and directly measured concentrations of chlorophyll were high, and some of the lowest yields were observed on 23 June, when [chl a] and chl_{rs} were very low (Figures 5–7). These extremes are the opposite of what would be expected if the chlorophyll-dependent effects on optical properties had been underestimated, suggesting that the large variability in F_{rs}^{abs} is real.

[51] To evaluate our model further, we explored the sensitivity of our results to the representation of chlorophyll-dependent effects on optical properties of phytoplankton (equation (17)). Recall that we held the term $\overline{a}_{\varphi}^{*}$ constant at an expected $\overline{a}_{\varphi}^{*}(512)$ for nanoplankton, and set Q_a^* to 1.0, characteristic of small cells, thereby underestimating the expected decrease of both their values with increasing chl_{rs} [*Bricaud et al.*, 1995; *Ciotti et al.*, 1999]. An implementation of our analysis with $a_{\varphi}^{*}(512)$ decreasing with increasing chl_{rs} according to *Bricaud et al.* [1995] (section 2.7.3; see Figure 9) shows that the magnitude of variability in fluorescence parameters is similar and general patterns with time are preserved for drifter eddy 1. Corresponding parameterization of Q_a^* as a function of chl_{rs} would accentuate the modest differences from our original analysis which assumed constant specific absorption and internal reabsorption coefficients. We conclude that unavoidable uncertainties in our estimation of the correction term, $[\overline{K}_{\mathrm{abs}}(\mathrm{chl}_{rs}) + \kappa_f(\mathrm{chl}_{rs})]/[\overline{a}_{\varphi}^{*}(\mathrm{chl}_{rs}) \cdot Q_a^*(\mathrm{chl}_{rs})]$, are not large enough to invalidate our assessment of the variability of F_{rs}^{abs} versus E and its relationship to inferred nutrient stress.

4.3.2. Eddy Dynamics and F^{abs} Versus Irradiance

[52] To explore possible relationships between SICF yield and nutrition as influenced by eddy dynamics over months, we determined how much of the variability in α_F^{abs} and $\phi_f(1500)$ for the drifters in the eddy could be explained statistically by variations in inferred nutrient availability dependent on the rotation period of the eddy. Figure 10 shows correlation coefficients between fluorescence parameters and the rotation period of the eddy, τ_{rot}, for drifter eddy 1. The correlations are calculated for different time lags between τ_{rot} and the respective fluorescence parameter because it is expected that the phytoplankton assemblage needs some time to acclimate to changes in nutrient supply. Maximum correlation coefficients of $r = 0.46$ for α_F^{abs} and $r = 0.52$ for $\phi_f(1500)$ are found for time lags between 3 and 4 days. Coefficients are $r = 0.53$ and $r = 0.59$, respectively, if $a_{\varphi}^{*}(512)$ is modeled as a function of chl_{rs} as described in section 4.3.1. The positive correlation with a positive lag indicates that slow rotation (i.e., reduced nutrient flux) corresponds to elevated values for α_F^{abs} and $\phi_f(1500)$ after a short lag, consistent with the findings of *Letelier et al.* [1997], who found a maximum cross correlation of 0.47 (reported SE = 0.045, $\alpha < 0.001$) with a lag of 0.87 days for the relationship of apparent quantum yield versus an inferred measure of nutrient availability in their eddy.

[53] Statistical significance of these correlations depends on the degrees of freedom, which will be smaller than the number of points ($n = 82-84$) because of autocorrelation within the time series. It is beyond the scope of this paper to determine the degrees of freedom in this case, in which the time series has already been subjected to detrending and filtering in an effort to establish the eddy rotation parameters. Variability on the order of 4 to 8 days, as observed in the chlorophyll record, suggests 20 to 10 degrees of freedom, respectively; maximum correlation coefficients in Figure 10 exceed the critical value for $\alpha = 0.05$ if d.f. = 20 but not if d.f. = 10.

4.3.3. F^{abs} Versus Irradiance and Independent Assessments of Nutrient Stress

[54] As with the study of *Letelier et al.* [1997], our statistical analysis relies on an inferred relationship between eddy dynamics and the input of nutrients to the photic zone. Significantly, we also have direct evidence of changing nutritional status of phytoplankton during the study (section 3.1 and Figure 7). On 11 June, a widespread bloom of phytoplankton was near its end, with direct measurements of *Fv*/*Fm* (0.407 ± 0.096 s.d., $n = 4$) indicating nutrient stress. By 23 June, the bloom had completely subsided; measurements of high *Fv*/*Fm* (0.600 ± 0.044 s.d., $n = 5$) suggest that a new, physiologically robust assemblage was established, with lower concentrations of biomass matched to the supply of nutrients. Measurements of F_{rs}^{abs} versus E for the two time periods contrast sharply (Figures 5 and 6): high fluorescence yield was associated with the independent indicator of nutrient stress and the apparently nutrient sufficient assemblages showed low fluorescence yields. This directly measured relationship between stress and increased SICF yield is identical to inferences reported by *Letelier et al.* [1997] and corroborated in section 4.3.2.

4.4. Physiological Model of Fluorescence Versus Irradiance

[55] Further research is required to determine if the relationship between fluorescence yield and nutritional status of phytoplankton, reported here and in one other study of an eddy [*Letelier et al.*, 1997], can form the basis of a more general diagnostic of the nutrient status of phytoplankton. It is possible, if not likely, that in many parts of the ocean, the fluorescence parameters α_F^{abs} and $\phi_f(1500)$ as estimated in this study are influenced strongly by physiological parameters other than nutrient status. For example, light history and acclimation of the phytoplankton should have some impact on the fluorescence properties [*Therriault et al.*, 1990; *Demmig-Adams et al.*, 1995; *Park et al.*, 1996; *Neale et al.*, 1998; *Laney et al.*, 2005]. Thus the mixing depth could be of importance when interpreting fluorescence parameters. Progress can be made if near-surface fluorescence versus irradiance parameters can be related directly to photosynthesis versus irradiance [e.g., *Babin et al.*, 1996; *Morrison*, 2003], the environmental control of which is better understood.

[56] Our improvements to the linear $\mathrm{FLH}/\mathrm{chl}_{rs}$ versus irradiance model of *Letelier et al.* [1997] not only enhance our confidence in the estimated parameters, they also allow us to explore variability in the quantum yield of fluorescence using an analytical model, equation (15), rather than proxies: we can now examine the relationships between ϕ_f and irradiance based on observations of ocean color from drifters and compare our results directly to studies of physiology, fluorescence and photosynthesis.

4.4.1. Mechanistic Model

[57] We adapted *Morrison*'s [2003] model describing the quantum yield of fluorescence as a function of irradiance to relate our estimates of $\phi_f = F_{rs}^{\mathrm{abs}}/\overset{\circ}{E}(\mathrm{PAR}, 0^-)$ to two processes that strongly influence fluorescence yield, photochemical and nonphotochemical quenching:

$$\phi_f = q_I \cdot \left[\phi_{fo} + \left(\phi_{f\max} - \phi_{fo}\right)\left(1 - e^{-E/E_{Kf}}\right)\right] \cdot e^{-E/E_T}, \quad (20)$$

where ϕ_{fo} and $\phi_{f\max}$ are the minimum and maximum quantum yields respectively, comparable to F_0 and F_m in

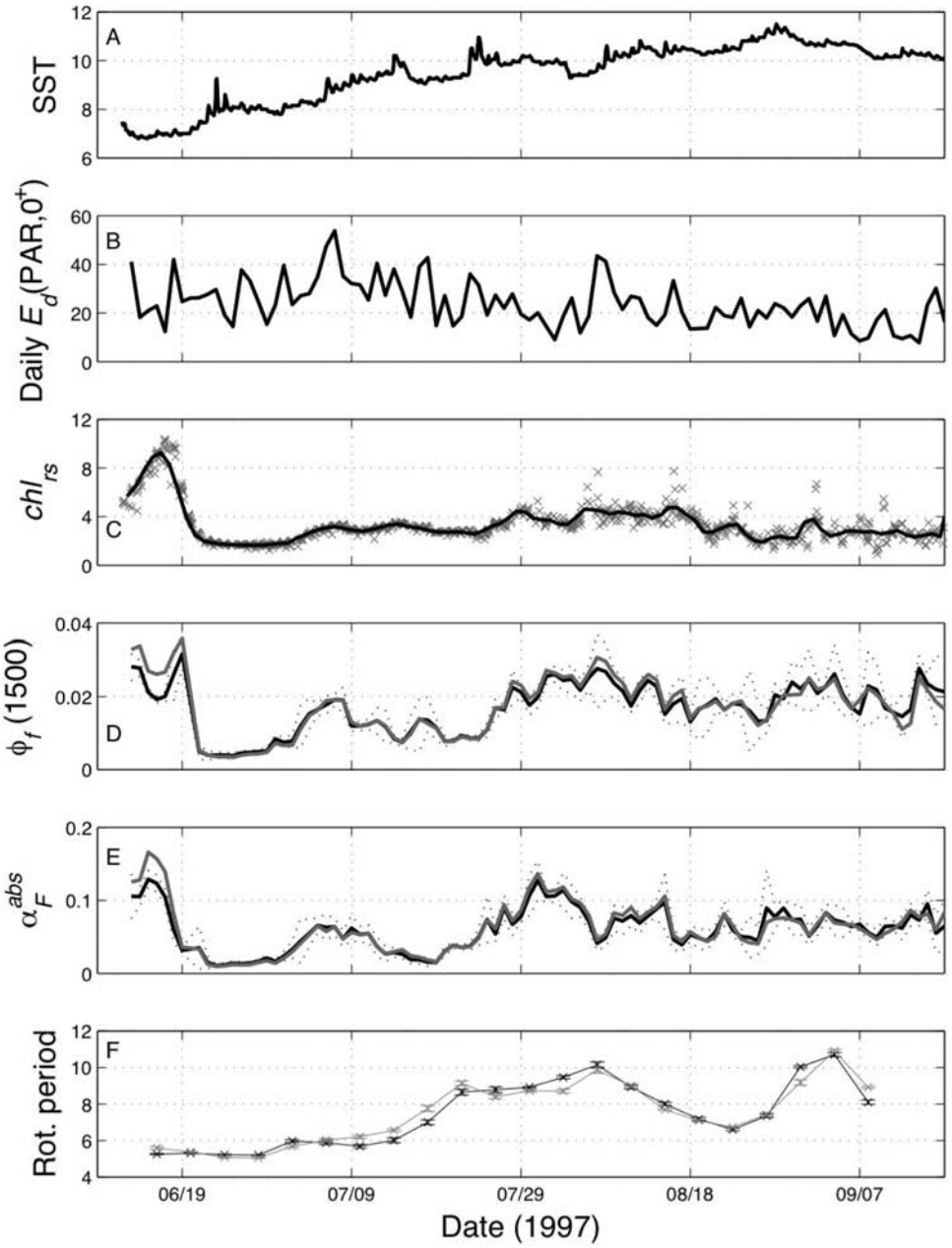

Figure 9. Time series plots for drifter eddy 1 and results from various analyses of the data. (a) Sea surface temperature, °C. (b) Integrated daily E_d(PAR, 0^+) (mol quanta m^{-2} d^{-1}). (c) Daily averaged chl_{rs} (mg m^{-3}), as indicated by the line; gray crosses indicate individual chl_{rs} estimates. (d, e) ϕ_f(1500) and α_F^{abs} (both dimensionless) estimated from curve fits. The black line shows parameters derived from curve fits, where the average phytoplankton specific absorption coefficient $a_\varphi^*(512)$ was kept constant; 95% confidence limits of these estimates are shown by the dotted line; the gray line indicates parameters from curve fits where $a_\varphi(512)$ varied with chl *a* concentrations following *Bricaud et al.* [1995]. (f) Rotation period of the eddy (crosses) with 95% error bars and connected for ease of visualization. The black line indicates estimates derived from north-south position, and the gray line stems from east-west position.

active fluorescence measurements [*Kiefer and Reynolds*, 1992] and E is the scalar irradiance (μmol quanta m^{-2} s^{-1}). The slow part of nonphotochemical quenching (order of hours to recover) [see, e.g., *Horton et al.*, 1996], is represented by q_I, which varies between 1 and 0 to represent minimal and maximal quenching, respectively. The parameters E_{Kf} and E_T (μmol quanta m^{-2} s^{-1}) scale the relationship with irradiance: E_{Kf} is the irradiance at which photochemical quenching approaches saturation and E_T is the irradiance above which energy-dependent nonphotochemical quenching (represented by q_E: section 4.4.3)

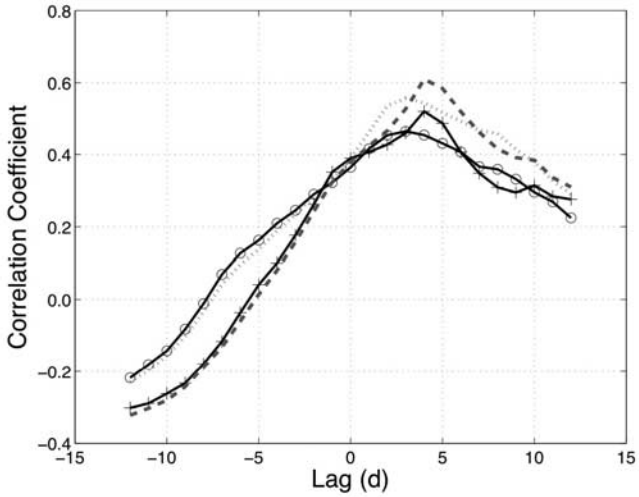

Figure 10. Correlation coefficients for the relationship between the rotation period of the eddy and α_F^{abs} (circles) and for correlations between the rotation period and $\phi_f(1500)$ (crosses); all data are from drifter eddy 1. The long-dashed and short-dashed gray curves show results for parameters that were derived from curve fits with $a_\varphi^*(512)$ modeled as a function of chl_{rs} (section 4.3.1); the short-dashed curve represents the correlations with α_F^{abs}, and the long-dashed curve shows correlations with $\phi_f(1500)$. The correlations were calculated for different time lags between the respective fluorescence parameter and the eddy's rotation period. A positive lag stands for the fluorescence parameter lagging the rotation period, and vice versa.

reaches its maximum [*Morrison*, 2003]. For the example presented here (Figure 11a), E_{Kf} and E_T are set at 100 μmol quanta m^{-2} s^{-1} and 1000 μmol quanta m^{-2} s^{-1}, respectively, to represent the typical shape of curves observed by the drifters. A dimensionless fraction, r, used by *Morrison* [2003] to represent reaction centers unaffected by nonphotochemical quenching, was omitted from our model, thereby eliminating an asymptotic nonzero quantum yield at very high irradiance that would yield nonsaturating relationships between F^{abs} and E similar to those in the model of *Laney et al.* [2005]. We examined the implications of the *Laney et al.* [2005] model, which relate primarily to the constancy of F^{abs} as irradiance increases, and found that they do not affect our conclusions about the mechanistic bases of variability in α_F^{abs} and $\phi_f(1500)$.

[58] Our model is used to examine possible effects of nutrient stress on the relationship between SICF and irradiance at the sea surface. Since ϕ_{fo} and $\phi_{f\,max}$ are comparable to F_0 and F_m in active fluorescence measurements, these parameters were used to simulate different levels of Fv/Fm, a recognized measure of physiological status of the phytoplankton [*Parkhill et al.*, 2001, and references therein]. The maximum quantum yield of fluorescence $\phi_{f\,max}$ was held constant at 0.09 and ϕ_{fo} was varied from 0.03 to 0.07, yielding Fv/Fm values between 0.67 and 0.22, corresponding to healthy nutrient replete, and nutrient stressed phytoplankton, respectively.

[59] The product of the fluorescence quantum yield and irradiance is equal to the realized fluorescence normalized to absorption (F^{abs} and its estimate F_{rs}^{abs}; see equation (7)), so we used the model results to generate curves of F^{abs} versus E (Figures 11b and 11d) that are directly comparable to our observations of F_{rs}^{abs} versus $\overset{o}{E}(PAR, 0^-)$ in Figure 5. The results are instructive.

4.4.2. Nutritional Status, Photochemical Quenching, and Fluorescence Versus Irradiance

[60] In healthy phytoplankton ($Fv/Fm = 0.67$; solid line in Figure 11a), photochemical quenching has a strong influence on the quantum yield of fluorescence for $E < E_{Kf}$, as shown by *Morrison* [2003] and others. Reduction of Fv/Fm to 0.22, consistent with nutrient stress, reveals the consequences of reduced photochemical quenching (dashed line in Figure 11a): fluorescence yield is more than doubled in low light. This is the well-recognized diagnostic of nutrient stress [*Kiefer*, 1973a; *Cleveland and Perry*, 1987] that forms the basis of the prediction that apparent quantum yield, i.e., the initial slope of the FLH/chl_{rs} versus E relationship, will be higher for nutrient-stressed phytoplankton assemblages [*Letelier et al.*, 1997]. Plots of F^{abs} versus E for the range of surface irradiance encountered in the Bering Sea (Figures 11b and 11d) show, however, that photochemical quenching has only a small influence on the relationship, contributing only to curvature near the origin. The initial slope of F^{abs} versus E is indeed influenced by photochemical quenching, thereby reflecting variations in Fv/Fm that are diagnostic of nutrient stress. But the changing F^{abs} versus E slope in low light might be barely discernible in records of FLH/chl_{rs} versus E or F_{rs}^{abs} versus $\overset{o}{E}(PAR, 0^-)$ for the broad range of surface irradiance recorded by drifters over the day at the surface. In fact, attempts to improve statistical fits to our data by accounting for photochemical quenching with a sigmoidal function were unsuccessful (section 2.8.1). Our statistical determination of initial slope (α_F^{abs} in equation (18)) thus mainly reflects the influence of processes other than photochemical quenching.

4.4.3. Energy-Dependent Nonphotochemical Quenching and F^{abs} Versus E

[61] The decline of fluorescence yield at high irradiance in Figure 11a can be attributed predominantly to energy-dependent nonphotochemical quenching, represented by the dimensionless q_E, equal to the final term in equation (20), $\exp(-E/E_T)$ [*Morrison*, 2003]. The consequence is an F^{abs} versus E curve similar in shape to commonly observed photosynthesis versus irradiance (P versus E) relationships [*Jassby and Platt*, 1976], providing support for our use of a typical P versus E form (equation (18)) for fitting F_{rs}^{abs} versus $\overset{o}{E}(PAR, 0^-)$ from the drifters. If E_T had been set much higher than its value of 1000 μmol quanta m^{-2} s^{-1}, the F^{abs} versus E function in Figure 11b would not saturate in the range of irradiance considered [cf. *Laney et al.*, 2005]; setting it lower would impose stronger inhibition of F^{abs} at high irradiance, generating a relationship between F^{abs} and E that would require an extra term to fit the data [cf. *Platt et al.*, 1980]. Nonsaturating behavior could also be produced by adding the factor r to equation (20), thereby reducing asymptotic inhibition as discussed in section 4.4.1. We conclude that *Morrison*'s [2003] model is suitable for describing a range of F^{abs} versus E relationships, including

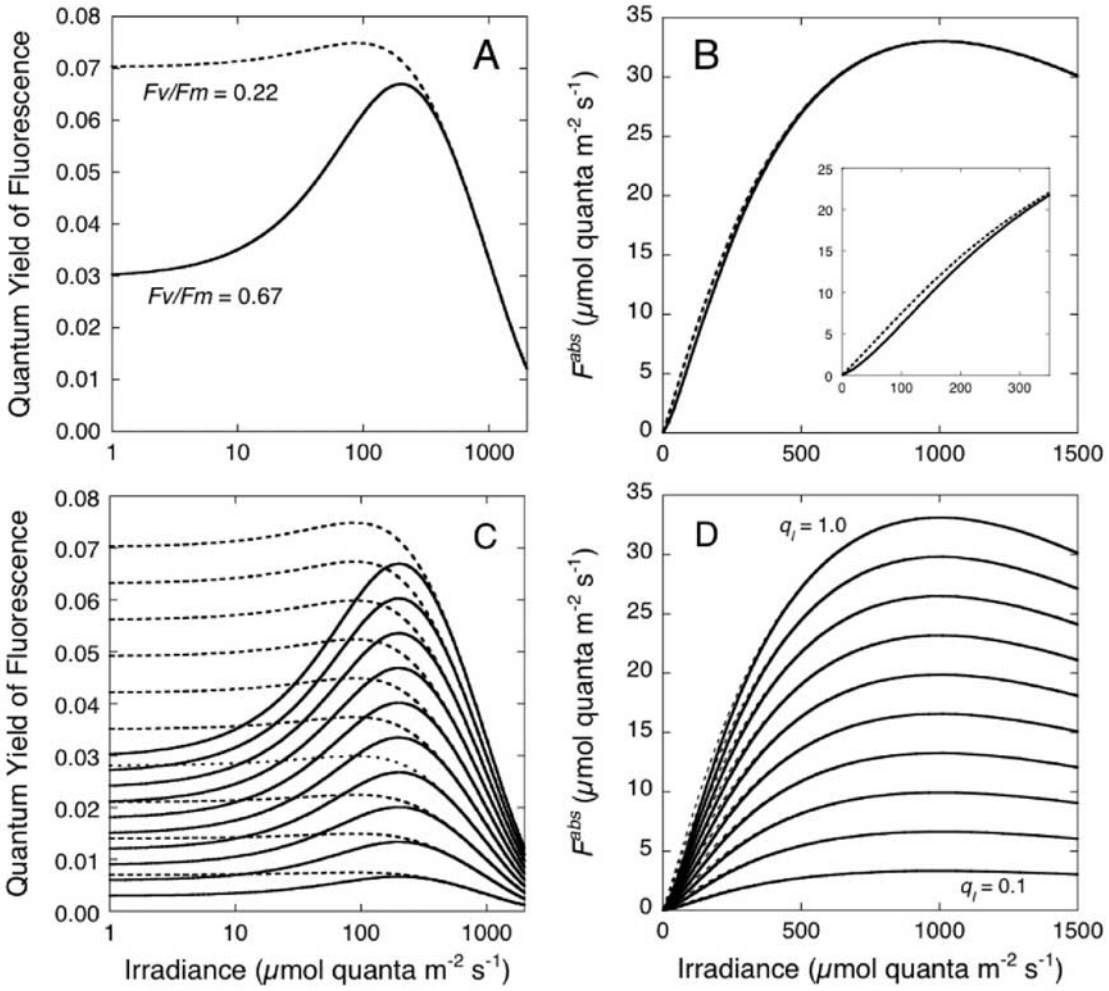

Figure 11. Relationships between fluorescence yield and irradiance from the modified model of *Morrison* [2003], equation (20). (a) Quantum yield of fluorescence (dimensionless) versus irradiance (log scale) for $Fv/Fm = 0.67$, consistent with unstressed, nutrient replete phytoplankton (solid line), and for $Fv/Fm = 0.22$, consistent with nutrient-stressed phytoplankton (dashed line). Photochemical quenching is responsible for the reduction of fluorescence yield at low irradiance, and energy-dependent nonphotochemical quenching leads to reductions at high irradiance. The slow component of nonphotochemical quenching, associated with both photoprotection and the inhibition of photosynthesis, is assumed to be absent: $q_I = 1.0$. (b) The product of quantum yield and irradiance, F^{abs} (μmol quanta m^{-2} s^{-1}), as a function of irradiance, from Figure 11a. The inset highlights differences in the initial slope of the relationship. (c) The same relationships as in Figure 11a, but for $q_I = 1.0$ (upper pair of curves; no slow quenching) in equal steps to $q_I = 0.1$ (lowest pair; very strong quenching). Compare these with *Morrison* [2003, Figure 9]. (d) F^{abs} versus irradiance for the pairs of curves in Figure 11c, illustrating that the effects of nutrition on photochemical quenching (solid versus dashed lines) are difficult to discern in relationships like these, which are dominated by nonphotochemical quenching and bear strong similarities to observations from the drifters in Figure 5.

the nonsaturating behavior in data presented by *Laney et al.* [2005].

[62] Our analysis of the effects of photochemical quenching and energy-dependent nonphotochemical quenching on fluorescence yield as a function of irradiance (equation (18) and Figure 11b) leads to an important conclusion: the initial slope of the F^{abs} versus E curve, α_F^{abs}, as determined by a relatively small number of measurements for irradiances between near zero and saturation of F^{abs}, reflects predominantly the maximum realized quantum yield and the effects of nonphotochemical quenching on fluorescence, not the effects of nutrition on photochemical quenching, which contribute to a curvature near the origin that is not likely to be detectable.

4.4.4. Slow Quenching, q_I, and F^{abs} Versus E

[63] The model of *Morrison* [2003] was cautiously designed to be consistent with research indicating that the slow component of nonphotochemical quenching decreased

fluorescence yield at all irradiances [*Krause and Weis*, 1991; *Demmig-Adams and Adams*, 1992; *Horton et al.*, 1996]. The process is accounted for with the dimensionless term q_I in our equation (20); its effect is illustrated in Figures 11c and 11d. The solid lines for nutrient replete phytoplankton in Figure 11c closely follow the model and data presented by *Morrison* [2003]; translation of the data to F^{abs} versus E in Figure 11d produces curves that can account for the wide variability of F_{rs}^{abs} versus $\overset{\circ}{E}(\mathrm{PAR}, 0^-)$ encountered during our study (Figures 5, 6, and 8), as well as the range of FLH/chl$_{rs}$ versus E slopes observed by *Letelier et al.* [1997], which encompassed a lower range of surface irradiance (maximum roughly 1000 μmol quanta m^{-2} s^{-1}). Because q_I is assumed to act equally at all irradiances, its effects dominate the gross patterns of F^{abs} versus E, masking the influences that nutrient stress may have on photochemical quenching. This does not exclude the possibility that nutrient stress can influence nonphotochemical quenching. For example, *Babin et al.* [1996] suggested that nutrient stress leads to damage of reaction centers and thus increased nonphotochemical quenching (reduced q_I [*Morrison*, 2003]). However, to reconcile the strong influence of q_I on F^{abs} versus E with our results of higher fluorescence yields associated with nutrient stress, we must invoke a physiological mechanism whereby the slow component of nonphotochemical quenching is somehow hampered in nutrient-stressed phytoplankton.

4.4.5. Magnitudes of Quantum Yields

[64] The variability of α_F^{abs} and $\phi_f(1500)$ as estimated from the drifters can be related to other estimates of the quantum yield of SICF at the surface [*Ostrowska et al.*, 1997; *Maritorena et al.*, 2000; *Morrison*, 2003], recently compared by *Huot et al.* [2005]. Briefly, α_F^{abs} as estimated here is a direct estimate of ϕ_f in relatively low light, i.e., dominated by its value at irradiances approaching, but not reaching saturation. These conditions are characteristic of mornings and late afternoons and cloudy days. The observed range of α_F^{abs}, mainly between about 0.01 and 0.1 (Figure 8), is roughly threefold higher than estimated ranges of $\phi_f(1500)$, which are more suitable for comparison with ϕ_f at the surface as observed by satellite sensors (0.003–0.03 [cf. *Huot et al.*, 2005]). We conclude that our estimates of SICF quantum yield and its variability, retrieved from ocean color drifters under sunny and cloudy conditions, are useful for comparison with and interpretation of variability in ϕ_f from satellite remote sensing.

5. Summary and Conclusions

[65] We developed a new approach to describe the relationship between Sun-induced chlorophyll fluorescence and solar irradiance near the sea surface. Estimates of fluorescence emission, corrected to account for optical properties of the water column and normalized to the absorption of light by pigments, were analyzed as a function of irradiance to describe variability of the quantum yield of fluorescence in bright sunlight typical for satellite observations ($\phi_f(1500)$) and under lower light as observed by drifters nearer to dawn and dusk and under clouds (α_F^{abs}). Fluorescence yields varied by a factor of 5 or more on the scale of days to weeks. We have related this variability directly to nutrient stress associated with the decline of a bloom, and indirectly to nutrient supply associated with dynamics of an eddy. In both cases, high fluorescence yield is associated with nutrient stress, just as *Letelier et al.* [1997] found in their study of fluorescence as measured by a drifter in the Southern Ocean.

[66] The well documented competition between photosynthesis and fluorescence for absorbed photons, i.e., photochemical quenching of fluorescence, has been invoked to explain increased fluorescence yield when nutrient stress impairs photosynthetic capabilities [e.g., *Kiefer*, 1973a; *Cleveland and Perry*, 1987; *Abbott et al.*, 2001]. The expectation, which we shared when beginning our analysis, was that photosynthetic debility would be revealed in higher initial slopes of the relationship between fluorescence, normalized to biomass, and irradiance (FLH/chl$_{rs}$ versus E [*Letelier et al.*, 1997]). But our analysis of the F^{abs} versus E relationship in a quantitative framework (after *Babin et al.* [1996], *Morrison* [2003], and *Huot et al.* [2005]), strongly suggests that both the initial slope, α_F^{abs}, and the quantum yield in bright light, $\phi_f(1500)$, were controlled by nonphotochemical quenching, the dissipation of excess absorbed radiation as heat, with concomitant reductions in quantum yields of both fluorescence and photosynthesis. Application of *Morrison*'s [2003] model suggests that energy-dependent quenching, represented by q_E, is the dominant influence on the shape of the F^{abs} versus E relationship, whereas the slow-to-recover q_I quenching, associated with inhibition of photosynthesis by excess irradiance [*Demmig-Adams and Adams*, 1992; *Horton et al.*, 1996], may explain the more than fivefold variation in both α_F^{abs} and $\phi_f(1500)$ that we observed. Thus, any hypothesis to explain the relationships between the physiological status of phytoplankton and Sun-induced fluorescence yield near the sea surface must invoke mechanistic links among environmental forcing, physiological state, and nonphotochemical quenching (q_E, q_I and possibly other processes) as a function of irradiance. Very little is known about these relationships. Carefully designed studies carried out in the laboratory and field should be able to shed light on the variations of α_F^{abs} and $\phi_f(1500)$ with light history, nonphotochemical quenching and nutrient status. Until new results are obtained, the apparent relationship between nutrient stress and high fluorescence yields near the sea surface will remain enigmatic. Pursuit of an explanation may lead the way to the use of Sun-induced fluorescence to diagnose the physiological status of phytoplankton from space.

Notation

$\overline{a}_\varphi$	absorption coefficient for phytoplankton, spectrally weighted for in situ irradiance over PAR, m^{-1}.
$\overline{a}_\varphi^*$	chlorophyll *a* specific absorption coefficient, spectrally weighted for in situ irradiance over PAR, m^2 (mg chl *a*)$^{-1}$.
$a_\varphi^*(\lambda)$	chlorophyll *a* specific absorption coefficient at wavelength λ, m^2 (mg chl *a*)$^{-1}$.
$a_w(683)$	absorption by water at 683 nm, m^{-1}.
$a_\varphi(683)$	absorption by phytoplankton at 683 nm, m^{-1}.

$A_{abs}(z)$ absorbed radiation at depth z, μmol quanta m^{-3} s^{-1}.
[chl a] concentration of chlorophyll a, mg chl m^{-3}.
chl_{rs} chlorophyll a concentration as estimated from remote sensing, mg chl m^{-3}.
ci 95% confidence interval.
C_f conversion factor for fluorescence, 26.6 nm.
E irradiance, μmol quanta m^{-2} s^{-1}.
$E_d(\lambda, 0^+)$ downwelling spectral irradiance above the surface, μmol quanta m^{-2} s^{-1} nm^{-1}.
$E_d(\mathrm{PAR}, 0^+)$ downwelling PAR irradiance above the surface, μmol quanta m^{-2} s^{-1}.
$\overset{o}{E}(\mathrm{PAR}, 0^-)$ scalar PAR irradiance just below the surface, μmol quanta m^{-2} s^{-1}.
E_{kF} saturation parameter for photochemical quenching, μmol quanta m^{-2} s^{-1}.
E_T scaling parameter for nonphotochemical quenching, μmol quanta m^{-2} s^{-1}.
E_b irradiance at the break point in the bilinear *Laney et al.* [2005] model, μmol quanta m^{-2} s^{-1}.
f Coriolis parameter, s^{-1}.
F fluorescence emission, μmol quanta m^{-3} s^{-1}.
F^{abs} fluorescence normalized to absorption, μmol quanta m^{-2} s^{-1}.
F^{abs}_{rs} fluorescence normalized to absorption and corrected for attenuation in the water column (from ocean color), μmol quanta m^{-2} s^{-1}.
F^{abs}_{max} maximum normalized fluorescence as estimated from the curve fits, μmol quanta m^{-2} s^{-1}.
F^{abs}_{1500} F^{abs}_{rs} at 1500 μmol quanta m^{-2} s^{-1}, μmol quanta m^{-2} s^{-1}.
Fv/Fm variable fluorescence, dimensionless.
FLH/chl_{rs} fluorescence line height normalized to estimated [chl a], μmol quanta m^{-2} s^{-1} nm^{-1} sr^{-1} (mg chl $m^{-3})^{-1}$.
$K_d(\lambda)$ diffuse attenuation coefficient, m^{-1}.
$\overline{K}_{abs}$ depth-averaged attenuation coefficient for absorbed radiation, m^{-1}.
L characteristic length scale, m.
$L_u(\lambda)$ upwelling radiance, μmol quanta m^{-2} s^{-1} nm^{-1} sr^{-1}.
$L_{ub}(\lambda)$ upwelling backscattered radiance, μmol quanta m^{-2} s^{-1} nm^{-1} sr^{-1}.
$L_{uf}(\lambda)$ upwelling fluoresced radiance, μmol quanta m^{-2} s^{-1} nm^{-1} sr^{-1}.
N Brunt-Väisälä frequency, s^{-1}.
PAR photosynthetically available radiation from 400 to 700 nm, μmol quanta m^{-2} s^{-1}.
q_E parameter representing energy-dependent nonphotochemical quenching, dimensionless.
q_I parameter representing the slow part of nonphotochemical quenching, dimensionless.
Q^*_a factor representing the emitted fluorescence not reabsorbed within the cell, dimensionless.
r radius, m.
$R(\lambda) = L_u(\lambda)/E_d(\lambda, 0^+)$, reflectance ratio, sr^{-1}.
Ri Richardson number, dimensionless.
Ro Rossby number, dimensionless.
$\Re$ transmission through the air-water interface, dimensionless.
t time, days.
T temperature, °C.
U characteristic velocity, m s^{-1}.
x distance from eddy center in north or east direction, m.
z depth, m.
Z_C critical value of the normalized Z value, dimensionless.
α^{abs}_F slope of the F^{abs} versus E curve, dimensionless.
β_1, β_2 initial and final slopes of the *Laney et al.* [2005] model, dimensionless.
ϕ phase, radians.
ϕ_f quantum yield of fluorescence, dimensionless.
ϕ_{fo} minimum quantum yield of fluorescence, dimensionless.
$\phi_{f\,max}$ maximum quantum yield of fluorescence, dimensionless.
$\phi_f(1500)$ ϕ_f estimated for $\overset{o}{E}(\mathrm{PAR}, 0^-) =$ 1500 μmol quanta m^{-2} s^{-1}, dimensionless.
κ_f attenuation coefficient for upwelling radiance at 683 nm, m^{-1}.
λ wavelength, nm.
ρ density, kg m^{-3}.
ρ_0 reference density, kg m^{-3}.
τ_{rot} period for a full rotation, days.
ω rotational velocity, d^{-1}.

[67] **Acknowledgments.** We thank Richard Davis for technical support and advice and Susanne Craig for comments on the manuscript. Ricardo Letelier provided important suggestions during the development of this study, one of which led to our recognition of nonphotochemical quenching as a dominant process. S. R. Laney made important suggestions for improved analysis; both he and J. R. Morrison provided many other helpful comments. The CTD data are courtesy of PMEL/NOAA, and we thank Phyllis Stabeno and Ned Cokelet, along with the captains and crews of R/V *Wecoma* and the NOAA ship *Ronald H. Brown*, for their cooperation. We thank J. P. Parkhill for the measurements of *Fv/Fm.* This work has been supported by PMEL/NOAA, NSERC Research Partnerships and Discovery Grants, the U.S. Office of Naval Research, NOPP, and CFCAS.

References

Abbott, M. R., and R. M. Letelier (1998), Decorrelation scales of chlorophyll as observed from bio-optical drifters in the California Current, *Deep Sea Res., Part II*, *45*, 1639–1667.

Abbott, M. R., and R. M. Letelier (1999), Algorithm theoretical basis document: Chlorophyll fluorescence (MODIS product number ATBD-MOD-22), NASA Goddard Space Flight Cent., Greenbelt, Md. (Available at http://modis.gsfc.nasa.gov/data/atbd/atbd_mod22.pdf)

Abbott, M. R., J. G. Richman, R. M. Letelier, and J. S. Bartlett (2000), The spring bloom in the Antarctic Polar Frontal Zone as observed from a mesoscale array of bio-optical sensors, *Deep Sea Res., Part II*, *47*, 3285–3314.

Abbott, M. R., J. G. Richman, J. S. Nahorniak, and B. S. Barksdale (2001), Meanders in the Antarctic Polar Frontal Zone and their impact on phytoplankton, *Deep Sea Res., Part II*, *48*, 3891–3912.

Babin, M., A. Morel, and B. Gentili (1996), Remote sensing of sea surface Sun-induced chlorophyll fluorescence: Consequences of natural variations in the optical characteristics of phytoplankton and the quantum yield of chlorophyll *a* fluorescence, *Int. J. Remote Sens.*, *17*, 2417–2448.

Balch, W. M., K. A. Kilpatrick, and C. C. Trees (1996), The 1991 coccolithophore bloom in the central North Atlantic: 1. Optical properties and factors affecting their distribution, *Limnol. Oceanogr.*, *41*, 1669–1683.

Behrenfeld, M. J., E. Boss, D. A. Siegel, and D. M. Shea (2005), Carbon-based ocean productivity and phytoplankton physiology from space, *Global Biogeochem. Cycles*, *19*, GB1006, doi:10.1029/2004GB002299.

Bricaud, A., M. Babin, A. Morel, and H. Claustre (1995), Variability in the chlorophyll-specific absorption coefficients of natural phytoplankton: Analysis and parameterization, *J. Geophys. Res.*, *100*, 13,321–13,332.

Chamberlin, W. S., C. R. Booth, D. A. Kiefer, J. H. Morrow, and R. C. Murphy (1990), Evidence for a simple relationship between natural fluorescence, photosynthesis and chlorophyll in the sea, *Deep Sea Res., Part A*, *37*, 951–973.

Chen, C., and O. L. Mangasarian (1996), A class of smoothing functions in nonlinear and mixed complementary problems, *Comput. Optim. Appl.*, *5*, 97–138.

Ciotti, Á. M., J. J. Cullen, and M. R. Lewis (1999), A semi-analytical model of the influence of phytoplankton community structure on the relationship between light attenuation and ocean color, *J. Geophys. Res.*, *104*, 1559–1578.

Ciotti, Á. M., M. R. Lewis, and J. J. Cullen (2002), Assessment of the relationships between dominant cell size in natural phytoplankton communities and the spectral shape of the absorption coefficient, *Limnol. Oceanogr.*, *47*, 404–417.

Cleveland, J. S., and M. J. Perry (1987), Quantum yield, relative specific absorption and fluorescence in nitrogen-limited *Chaetoceros gracilis*, *Mar. Biol.*, *94*, 489–497.

Cullen, J. J., and R. F. Davis (2003), The blank can make a big difference in oceanographic measurements, *Limnol. Oceanogr.*, *12*, 29–35.

Cullen, J. J., and M. R. Lewis (1995), Biological processes and optical measurements near the sea-surface: Some issues relevant to remote sensing, *J. Geophys. Res.*, *100*, 13,255–13,266.

Cullen, J. J., Á. M. Ciotti, R. F. Davis, and P. J. Neale (1997), The relationship between near-surface chlorophyll and solar-stimulated fluorescence: Biological effects, *Proc. SPIE Ocean Opt. Eng.*, *XIII*, 272–277.

Culver, M. E., and M. J. Perry (1997), Calculation of solar-induced fluorescence in surface and subsurface waters, *J. Geophys. Res.*, *102*, 10,563–10,572.

Demmig-Adams, B., and W. W. Adams III (1992), Photoprotection and other responses of plants to high light stress, *Annu. Rev. Plant Physiol. Plant Mol. Biol.*, *1992*, 599–626.

Demmig-Adams, B., W. W. Adams III, B. A. Logan, and A. S. Verhoeven (1995), Xanthophyll-cycle-dependent energy dissipation and flexible photosystem II efficiency in plants acclimated to light stress, *Aust. J. Plant Physiol.*, *22*, 249–260.

Falkowski, P. G., and D. A. Kiefer (1985), Chlorophyll *a* fluorescence in phytoplankton: Relationship to photosynthesis and biomass, *J. Plankton Res.*, *7*, 715–731.

Falkowski, P. G., and Z. Kolber (1995), Variations in chlorophyll fluorescence yields in phytoplankton in the world oceans, *Aust. J. Plant Physiol.*, *22*, 341–355.

Falkowski, P. G., D. Ziemann, Z. Kolber, and P. K. Bienfang (1991), Nutrient pumping and phytoplankton response in a subtropical mesoscale eddy, *Nature*, *352*, 544–551.

Franks, P. J. S., J. S. Wroblewski, and G. R. Flierl (1986), Prediction of phytoplankton growth in response to the frictional decay of a warm-core ring, *J. Geophys. Res.*, *91*, 7603–7610.

Gill, A. E. (1982), *Atmosphere-Ocean Dynamics*, Academic, New York.

Gilmore, A. M., and Govindjee (1999), How higher plants respond to excess light: Energy dissipation in photosystem II, in *Concepts in Photobiology: Photosynthesis and Photomorphogenesis*, edited by G. S. Singhal et al., pp. 513–548, Narosa, New Delhi.

Gordon, H. R. (1979), Diffuse reflectance of the ocean: The theory of its augmentation by chlorophyll *a* fluorescence, *Appl. Opt.*, *18*, 1161–1166.

Hitchcock, G. L., A. J. Mariano, and T. Rossby (1993), Mesoscale pigment fields in the Gulf Stream: Observations in a meander crest and trough, *J. Geophys. Res.*, *98*, 8425–8445.

Horton, P., A. V. Ruban, and R. G. Walters (1996), Regulation of light harvesting in green plants, *Annu. Rev. Plant Physiol. Plant Mol. Biol.*, *47*, 655–684.

Huber, P. J. (1981), *Robust Statistics*, 308 pp., John Wiley, New York.

Huot, Y., C. A. Brown, and J. J. Cullen (2005), New algorithms for MODIS Sun-induced chlorophyll fluorescence and a comparison with present data products, *Limnol. Oceanogr.*, *3*, 108–130.

Huot, Y., C. A. Brown, and J. J. Cullen (2007), Retrieval of phytoplankton biomass from simultaneous inversion of reflectance, the diffuse attenuation coefficient, and Sun-induced fluorescence in coastal waters, *J. Geophys. Res.*, *112*, C06013, doi:10.1029/2006JC003794.

Jassby, A. D., and T. Platt (1976), Mathematical formulation of the relationship between photosynthesis and light for phytoplankton, *Limnol. Oceanogr.*, *21*, 540–547.

Jerome, J. H., R. P. Bukata, and J. E. Bruton (1988), Utilizing the components of vector irradiance to estimate the scalar irradiance in natural waters, *Appl. Opt.*, *27*, 4012–4018.

Kiefer, D. A. (1973a), Chlorophyll *a* fluorescence in marine centric diatoms: Responses of chloroplasts to light and nutrient stress, *Mar. Biol.*, *23*, 39–46.

Kiefer, D. A. (1973b), Fluorescence properties of natural phytoplankton assemblages, *Mar. Biol.*, *22*, 263–269.

Kiefer, D. A., and R. A. Reynolds (1992), Advances in understanding phytoplankton fluorescence and photosynthesis, in *Primary Productivity and Biogeochemical Cycles in the Sea*, edited by P. G. Falkowski and A. Woodhead, pp. 155–174, Plenum, New York.

Kiefer, D. A., W. S. Chamberlin, and C. R. Booth (1989), Natural fluorescence of chlorophyll *a*: Relationship to photosynthesis and chlorophyll concentration in the western South Pacific gyre, *Limnol. Oceanogr.*, *34*, 868–881.

Kirk, J. T. O. (1994), *Light and Photosynthesis in Aquatic Ecosystems*, 2nd ed., 509 pp., Cambridge Univ. Press, New York.

Knauss, J. A. (1996), *Introduction to Physical Oceanography*, 2nd ed., Prentice-Hall, Upper Saddle River, N. J.

Krause, G. H., and E. Weis (1991), Chlorophyll fluorescence and photosynthesis: The basics, *Annu. Rev. Plant Physiol. Plant Mol. Biol.*, *42*, 313–349.

Landry, M. R., et al. (1997), Iron and grazing constraints on primary production in the central equatorial Pacific: An EqPac synthesis, *Limnol. Oceanogr.*, *42*, 405–418.

Laney, S. R., R. M. Letelier, and M. R. Abbott (2005), Parameterizing the natural fluorescence kinetics of *Thalassiosira weissflogii*, *Limnol. Oceanogr.*, *50*, 1499–1510.

Lee, M.-M., and R. G. Williams (2000), The role of eddies in the isopycnic transfer of nutrients and their impact on biological production, *J. Mar. Res.*, *58*, 895–917.

Letelier, R. M., M. R. Abbott, and D. M. Karl (1997), Chlorophyll natural fluorescence response to upwelling events in the Southern Ocean, *Geophys. Res. Lett.*, *24*, 409–412.

Letelier, R. M., D. M. Karl, M. R. Abbott, P. Flament, M. Freilich, R. Lukas, and T. Strub (2000), Role of late winter mesoscale events in the biogeochemical variability of the upper water column of the North Pacific Subtropical Gyre, *J. Geophys. Res.*, *105*, 28,723–28,793.

Lévy, M. (2003), Mesoscale variability of phytoplankton and of new production: Impact of the large scale nutrient distribution, *J. Geophys. Res.*, *108*(C11), 3358, doi:10.1029/2002JC001577.

Lévy, M., P. Klein, and A.-M. Treguier (2001), Impact of sub-mesoscale physics on production and subduction of phytoplankton in an oligotrophic regime, *J. Mar. Res.*, *59*, 535–565.

Lewis, M. R. (2002), Variability of plankton and plankton processes on the mesoscale, in *Phytoplankton Productivity: Carbon Assimilation in Marine and Freshwater Ecosystems*, edited by P. J. L. Williams et al., pp. 141–155, Blackwell, Oxford, U. K.

Lohrenz, S. E., J. J. Cullen, D. A. Phinney, D. B. Olson, and C. S. Yentsch (1993), Distributions of pigments and primary production in a Gulf Stream meander, *J. Geophys. Res.*, *98*, 14,545–14,560.

Longhurst, A. R. (2007), *Ecological Geography of the Sea*, 2nd ed., 542 pp., Academic, San Diego, Calif.

Maritorena, S., A. Morel, and B. Gentili (2000), Determination of the fluorescence quantum yield by oceanic phytoplankton in their natural habitat, *Appl. Opt.*, *39*, 6725–6737.

Martin, A. P., and K. J. Richards (2001), Mechanisms for vertical nutrient transport within a North Atlantic mesoscale eddy, *Deep Sea Res., Part II*, *48*, 757–773.

McGillicuddy, D. J., Jr., et al. (2007), Eddy/wind interactions stimulate extraordinary mid-ocean plankton blooms, *Science*, *316*, 1021–1026.

McGowan, J. A. (2004), Sverdrup's biology, *Oceanogr. Mag.*, *17*, 106–112.

Morrison, J. R. (2003), In situ determination of the quantum yield of phytoplankton chlorophyll a fluorescence: A simple algorithm, observations, and a model, *Limnol. Oceanogr.*, *48*, 618–631.

Müller, P., X.-P. Li, and K. N. Niyogi (2001), Non-photochemical quenching: A response to excess light energy, *Plant Physiol.*, *125*, 1558–1566.

National Research Council (1996), *The Bering Sea Ecosystem*, 324 pp., Natl. Acad. Press, Washington, D. C.

Neale, P. J., J. J. Cullen, and R. F. Davis (1998), Inhibition of marine photosynthesis by ultraviolet radiation: Variable sensitivity of phytoplankton in the Weddell-Scotia Sea during austral spring, *Limnol. Oceanogr.*, *43*, 433–448.

O'Reilly, J. E., S. Maritorena, B. G. Mitchell, D. A. Siegel, K. L. Carder, S. A. Garver, M. Kahru, and C. R. McClain (1998), Ocean color chlorophyll algorithm for SeaWiFS, *J. Geophys. Res.*, *103*, 24,937–24,953.

Ostrowska, M., M. Darecki, and B. Wozniak (1997), An attempt to use measurements of Sun-induced chlorophyll fluorescence to estimate chlorophyll a concentration in the Baltic Sea, *Proc. SPIE Int. Soc. Opt. Eng.*, *3222*, 528–537.

Park, Y.-I., W. S. Chow, J. M. Anderson, and V. M. Hurry (1996), Differential susceptibility of Photosystem II to light stress in light-acclimated pea leaves depends on the capacity for photochemical and non-radiative dissipation of light, *Plant Sci.*, *115*, 137–149.

Parkhill, J.-P., G. Maillet, and J. J. Cullen (2001), Fluorescence-based maximal quantum yield for PSII as a diagnostic of nutrient stress, *J. Phycol.*, *37*, 517–529.

Parks, T. W., and C. S. Burrus (1987), *Digital Filter Design*, John Wiley, New York.

Pérez, F. F., M. Gil-Coto, and A. F. Ríos (2003), Large and mesoscale variability of the water masses and the deep chlorophyll maximum in the Azores Front, *J. Geophys. Res.*, *108*(C7), 3215, doi:10.1029/2000JC000360.

Platt, T., C. L. Gallegos, and W. G. Harrison (1980), Photoinhibition of photosynthesis in natural assemblages of marine phytoplankton, *J. Mar. Res.*, *38*, 687–701.

Pope, R. M., and E. S. Fry (1997), Absorption spectrum (380–700 nm) of pure water: II. Integrating cavity measurements, *Appl. Opt.*, *36*, 8710–8723.

R Development Core Team (2007), *R: A Language and Environment for Statistical Computing*, R Found. for Stat. Comput., Vienna, Austria.

Samuelsson, G., and G. Öquist (1977), A method for studying photosynthetic capacities of unicellular algae based on in vivo chlorophyll fluorescence, *Plant Physiol.*, *40*, 315–319.

Springer, A. M., C. P. McRoy, and M. V. Flint (1996), The Bering Sea Green Belt: Shelf-edge processes and ecosystem production, *Fish. Oceanogr.*, *5*, 205–223.

Strickland, J. D. H., and T. R. Parsons (1972), A practical handbook of seawater analysis, *J. Fish. Res. Board Can.*, *167*, 1–310.

Sverdrup, H. U. (1955), The place of physical oceanography in oceanographic research, *J. Mar. Res.*, *14*, 287–294.

Therriault, J.-C., D. Booth, L. Legendre, and S. Demers (1990), Phytoplankton photoadaptation to vertical excursion as estimated by an in vivo fluorescence ratio, *Mar. Ecol. Prog. Ser.*, *60*, 97–111.

Topliss, B. J. (1985), Optical measurements in the Sargasso sea: Solar stimulated chlorophyll fluorescence, *Oceanol. Acta*, *8*, 263–270.

Tranter, D. J., R. R. Parker, and G. R. Cresswell (1980), Are warm-core eddies unproductive?, *Nature*, *284*, 540–542.

Venables, W. N., and B. D. Ripley (1994), *Modern Applied Statistics with S*, 3rd ed., 495 pp., Springer, New York.

Williams, R. G., and M. J. Follows (2003), Physical transport of nutrients and the maintenance of biological production, in *Ocean Biogeochemistry: A JGOFS Synthesis*, edited by M. Fasham, pp. 19–50, Springer, New York.

Yentsch, C. S., and J. C. Garside (1986), Patterns of phytoplankton abundance and biogeography, in *Pelagic Biogeography*, edited by A. C. Pierrot-Bults et al., pp. 278–284, UNESCO, Paris.

Yentsch, C. S., and D. A. Phinney (1985), Rotary motions and convection as a means of regulating primary production in warm core rings, *J. Geophys. Res.*, *90*, 3237–3248.

J. J. Cullen, D. E. Kelley, M. R. Lewis, and C. Schallenberg, Department of Oceanography, Dalhousie University, 1355 Oxford Street, Halifax, NS, Canada B3H 4J1. (john.cullen@dal.ca)